KINETICS OF DISCONTINUOUS COARSENING OF CELLULAR PRECIPITATE IN AN Al - 20 at% Zn ALLOY

by

V. SURESH

DEPARTMENT OF METALLURGICAL ENGINEERING
INDIAN INSTITUTE OF TECHNOLOGY, KANPUR

MAY, 1985

KINETICS OF DISCONTINUOUS COARSENING OF CELLULAR PRECIPITATE IN AN Al - 20 at% Zn ALLOY

A Thesis Submitted
In Partial Fulfilment of the Requirements
for the Degree of
MASTER OF TECHNOLOGY

by
V. SURESH

to the

DEPARTMENT OF METALLURGICAL ENGINEERING
INDIAN INSTITUTE OF TECHNOLOGY, KANPUR

MAY, 1985

ME-1985-M-SUR-KIN

CERTIFICATE

This is to certify that the M.Tech. thesis entitled, ''KINETICS OF DISCONTINUOUS COARSENING OF CELLULAR PRECIPITA IN AN Al-20 at Zn ALLOY'' by V. Suresh has been carried ou under my supervision and that the same has not been submitte elsewhere for a degree.

May 14th, 1985

(S.P. GUPTA)
Assistant Professo
Dept. of Met. Engg
I.I.T., Kanpur

CONTENTS

		Page
LIST OF TABLES		vi)
LIST OF FIGURES		vii)
ABSTRACT		viii)
CHAPTER 1 :	INTRODUCTION	
1.1 :	Discontinuous Precipitation, General	2
1.2 :	Morphology of Cellular Reaction	3
1.3 :	Aluminum-Zinc System	6
1.4 :	Models for Kinetics of Discontinuous Precipitation	10
	1.4.1 Turnbull's Model	10
	1.4.2 Aaronson and Liu Treatment	12
	1.4.3 Cahn's Treatment	13
	1.4.4 Petermann and Hornbogen's Treatment of Cellular Precipitation	15
	1.4.5 Shapiro and Kirkaldy's Analysis	17
	1.4.6 Sundquist's Analysis	18
	1.4.7 Petermann and Hornbogen's Theory of Discontinuous Coarsening	19
CHAPTER 2 :	EXPERIMENTAL PROCEDURE	
2.1 :	Alloy Preparation	21
2.2 :	Heat Treatment of the Alloy	21
2.3 :	Examination of the Treated Specimens	22
	2.3.1 Optical Microscopic Examination	22
	2.3.2 Transmission Electron Microscope Examination	22
2.4 :	X-ray Analysis	23
CHAPTER 3 :	RESULTS AND DISCUSSION	
3.1 :	Growth Rate	24
3.2 :	Interlamellar Spacing	28
3.3 :	Composition of the Depleted Matrix	32
3.4 :	Calculation of the Driving Force for Cellular Precipitation	36
3.5 :	Kinetics of Primary Cellular Reaction	44

		Page
3.6	: Kinetics of Discontinuous Coarsening: Secondary Reaction	51
3.7	: Morphology of Cellular Precipitate	56
CHAPTER 4	: CONCLUSIONS	
references		66

LIST OF TABLES

Table	Title	Page
1	Growth rate, Interlamellar spacing and composition data of primary and secondary cell growth	27
2	Chemical free energy and surface free energy associated with primary and secondary reaction	42
3	Free energy values calculated from the data of Hilliard et.al.(33)	43
4	D_b δ for primary and secondary cell growth	49
5	Activation energy, diffusivity and D_o values for different theories	50
6	Temperature - Fraction of driving force used for precipitation data	55

LIST OF FIGURES

Figure	Title	Page
1	Aluminum-zinc Phase diagram	7
2	Growth rate vs. temperature	25
3	Interlamellar spacing (s) vs. temperature	29
4	S vs ΔT	31
5	Lattice Parameter vs. Composition	33
6	Composition of depleted matrix vs. temperature	34
7	S^M vs. composition	37
	H^M vs. Composition	37
8	Change in free energy ΔG vs. temperature	38
9.	Free energy-composition diagram at 350°K	39
10	Free energy-composition diagram at 460°K	40
11	$D_b\,\delta$ vs $1/T$ (Primary reaction)	45
12	$D_b\,\delta$ vs $1/T$ (Primary reaction)	46
13	$D_b\,\delta$ vs $1/T$ (Secondary reaction)	52
14	Fraction of driving force (P) vs. temperature	54
15	TEM Photograph of Primary Lamellae	60
16	TEM Photograph of Secondary lamellae	60
17	Microstructure of as quenched sample	61
18	Room temperature ageing sequence of a quenched sample	62
19	Formation of grain boundary precipitate	63

ABSTRACT

The primary discontinuous precipitation and coarsening were studied in Al 20 at% Zn alloy at a wide range of ageing temperatures, ranging from 350°K to 500°K. The techniques used for the investigation included optical microscopy, Transmission electron microscopy and x-ray diffraction. The growth kinetics of both primary and secondary reactions were investigated by calculating the driving force for the reaction.

The model proposed by Petermann and Hornbogen is found to be most suitable for both Primary and secondary reactions for the entire range of temperature. The growth kinetics of primary reaction was investigated using other models proposed by Cahn, Turnbull, Aaronson and Liu, Sundquist, Shapiro and Kirkaldy. The model proposed by Petermann and Hornbogen is based on the assumption that the driving force for the coarsening reaction is contributed from the remaining free energy after the primary reaction.

It is also seen that the value of D_b calculated from the results obtained in this study are higher than the corresponding values of diffusivity of zinc in Aluminum (D_v), at the same range of temperature. This clearly shows that the cellular reaction is controlled by grain boundary diffusion of zinc.

The morphological features of the primary and secondary precipitate were studied. It was observed that the Primary precipitate~~s~~ nucleates at the grain boundaries of supersaturated solid solution even while ageing at room temperature. The moving reaction front (cell-matrix interface) leaves behind alternate lamellae of depleted α and ~~β~~ zinc rich β phase. The secondary precipitate is observed at the original grain boundaries and at the impinged regions of a two primary cell-matrix interfaces. Further growth occurs by the migration of the nucleated boundary into the opposite grain. The growth rate of secondary cell interface is ~~are~~ much slower compared to that of Primary cells, as a result of which the secondary cells have a larger value of interlamellar spacing than the primary.

CHAPTER 1

INTRODUCTION

The phenomenon of discontinuous coarsening of the cellular precipitate has been studied in a few alloy systems (1,2,3,4). Although the morphology of the reaction is well understood, very little development has taken place in establishing the kinetics of coarsening or secondary reaction. The earliest theory for the secondary reaction was proposed by Livingston and Cahn (5), which states that the driving force for secondary reaction comes from the decrease in the interfacial energy (of the α/β interface) accompanying the coarsening reaction. However the theory does not use the available chemical free energy as the driving force. As a result of this factor the kinetics of the reaction fails to follow this model at higher temperatures.

A theory was proposed by Fournelle (1) to overcome the shortcomings of the earlier theory of Livingstone and Cahn (5). This is an extension of the theory proposed by Petermann and Hornbogen (7) for the primary cellular reaction. This model is based on Lücke's theory (6) of boundary migration. According to this theory the driving force for the secondary reaction comes from the free energy not used in the primary reaction.

The present investigation was carried out in an Al-20 at% Zn alloy. The kinetics of coarsening of the cellular precipitate was analysed using the above theories. Simultaneously the kinetics of the primary reaction was also analysed using theories proposed by Cahn (8), Turnbull (9), Aaronson and Liu (10), Petermann and Hornbogen (7), Sundiquist (11) and Shapiro and Kirkaldy (12).

1.1 Discontinuous Precipitation, General

The segregation of solute from a supersaturatedsolid solution into two phases occurs by cellular mode when the boundary between two adjacent grains of the original solid solution becomes unstable and starts to migrate (13). As the boundary migrates, a solute rich precipitate and depleted solid solution ~~is~~ are formed behind the advancing interface. The initiation of this type has been studied in great detail (14,15). However, it has not been possible to conclude the exact reasons for the occurrence of this type of a reaction in certain systems. Hornbogen (16) made a study of the cellular reaction and has stated some important factors that favour discontinuous precipitation. These include high probability of heterogeneous nucleation at the grain boundaries as compared to nucleation inside the grain, a high grain boundary diffusion coefficient and a high driving force for precipitation. Apart from these major factors he has also analysed the nature of the structure of

grain boundary during the cellular reaction as it affects the grain boundary diffusivity value.

Meyrick (17), in his study on the initiation of discontinuous precipitation states that the grain boundary provides the passage for the diffusional processes whereby the compositional changes are effected as the boundary advances. It can be inferred that for alloys in which the solute is likely to segregate at the grain boundaries, thereby reducing the energy of the grain boundary, a diminition in segregated population due to precipitation can provide the driving force for the boundary to migrate. Meyrick concludes that the degree of solute segregation of the grain boundary is one of the distingushing factors between alloys in which discontinuous precipitation can occur and those in which it does not occur.

1.2 Morphology of Cellular Reaction

The earliest studies (14,18,19) on cellular reactions were aimed ~~in~~ at the morphology of the cellular precipitate and the initiation of the reaction. It is very evident that in most cellular reactions the supersaturated solid solution decomposes into a solute depleted matrix having the crystal structure of the original solid solution and solute rich precipitate phase. These form as alternate lamellae of α and β extending all the way from the interface into the matrix.

These are characterised by definite value of interlamellar-spacing, which in turn depends on the ageing temperature. One of the early mechanisms proposed for the initiation of cellular precipitation was by Tu and Turnbull (14). This is commonly referred as the 'Pucker' mechanism. Here the precipitate initiation begins with the nucleation, on one side of the grain boundary, of a disc or plate shaped precipitate having a high energy (incoherent) interface across the boundary and a low energy interface with the grain in which it is embedded. The orientation of the precipitate, necessary to bring the low energy habit plane between precipitate and matrix grain into alignment is assumed to result in the local deflection of the boundary into a puckered configuration. This causes a movement of the grain boundary thereby leaving the precipitate embedded in the grain. However, one side of the precipitate is attached to the tip of the boundary. The initial driving force for the boundary migration is provided by the reduction in interfacial energy of the precipitate. This has been the operating mechanism in Pb-Sn alloys (14).

In some alloy systems exhibiting cellular precipitation such as Fe-Zn, (18), Cu-In (15) no definite habit and orientation relationship appears to exist for the precipitate phase and the depleted matrix phase, and lamellae appear to have the ability to change direction and branch. Under these

circumstances Tu and Turnbull mechanism fails to describe the genesis of cellular precipitate. Fournelle and Clark (15) proposed a mechanism taking into account the above problem. In their analysis (15), it is reported that when kept at a suitable temperature, the grain boundary migrates at measurable rates like the grain boundary migration during normal grain growth. The migrating boundary interacts with the solute that come across it. This leads to the formation of allotriomorphs. Nucleation of similarly oriented lamellae in neighbouring regions leads to the formation of cells. It is also mentioned that the crystallographic habit and orientation of the initial allotriomorphs appear to have little influence on the final cell structure.

It has been found that products of primary cellular reaction to be decomposed by secondary cellular reaction (20,29,30). The decomposition takes place by migration of secondary cell boundary into the products of the Primary reaction. It has also been observed that the growth rates are much slower compared to the rates during the primary reaction and thereby the secondary inter lamellar spacing is much higher compared to the Primary reaction. The morphology of the secondary reaction has been studied in many alloy systems (2,3,4,20,30). Fournelle (20) has proposed a mechanism known as the 'S' mechanism to explain the morphology of secondary reaction. Here the adjacent

segments of two supersaturated grains are found to migrate into opposite grains leaving behind cellular lamellae oriented with respect to the grain from which they originated. Continuing this growth they intersect at a common point on the original grain boundary in such a way that the advancing boundary of each cell finally grows into the origin of its counterpart at the original grain boundary and decomposition of Primary lamellae by secondary reaction starts taking place. It has also been observed that the intersection of two primary cells acts as a site for the start of secondary reaction. Also, the secondary cells originate at the primary cell-grain boundary intersections.

1.3 Aluminum-Zinc System (19)

The Aluminum-Zinc equilibrium phase diagram is shown in Fig.1. It is an extensive solid solution of zinc in aluminum, with the solid solution range extending upto 66 at % Zn. This solid solution occurs in three different forms of FCC structure namely α, α', γ. There are principally two monotectoid reactions (1) $\alpha' \longrightarrow \alpha + \gamma$, concerned with three isostructural phases, (ii) $\alpha' \longrightarrow \alpha + \beta$ where a aluminum rich FCC phase and zinc-rich hexagonal β form at room temperature.

In the past two decades the decomposition of Al-Zn alloys over a wide range of composition has been studied in great detail (21,22,23,24,25,27,28). However, these

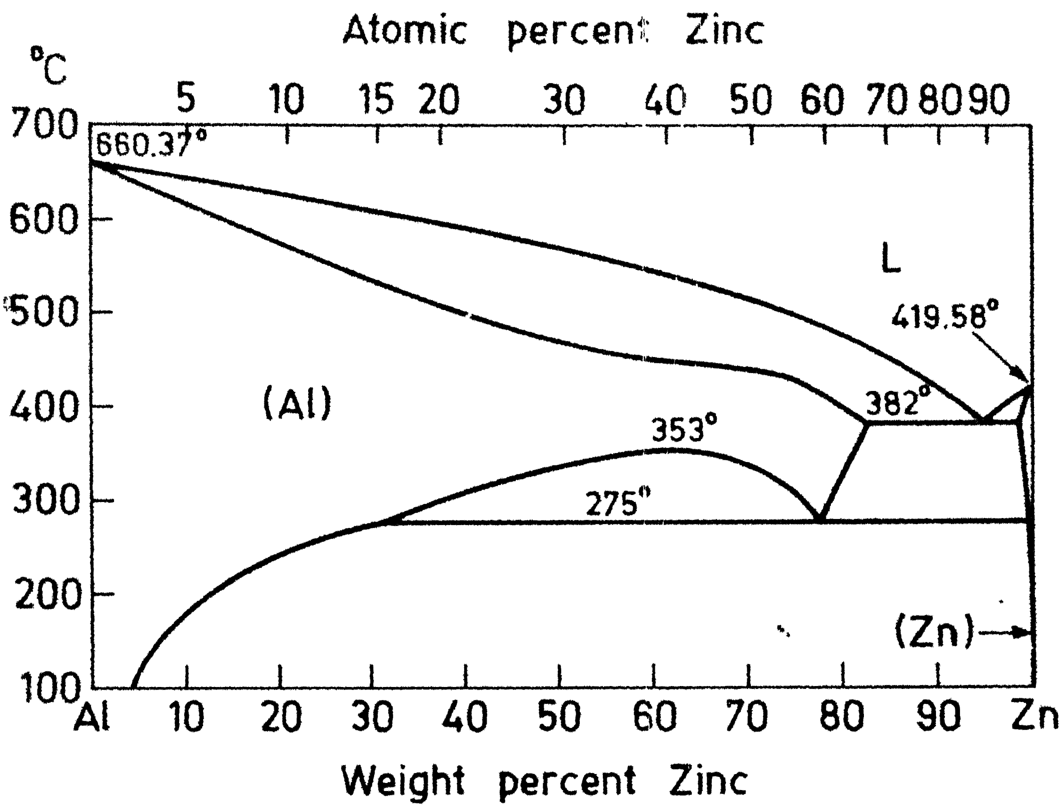

Fig. 1 Aluminium-Zinc phase diagram (19)

studies were confined to either spinodal decomposition characteristics (28) or the study of the metastable transition phases viz. G.P.Zones, Rhombohedral R phase. The precipitation sequence during the decomposition of quenched Al-Zn alloy is well established. It is as follows -

$$\text{Supersaturated } (\alpha) \xrightarrow[\text{temperature}]{\text{Quench to room}} \text{G.P.Zones} \text{ — Rhombohedral } ' \text{ Hexagonal Zinc } (\beta)$$

The main objective of this investigation is to study the kinetics of cellular transformation Al-Zn alloy. There has been a number of investigations in the recent past on the growth kinetics of cellular transformation in Al-Zn alloys for a wide range of composition from 15 at % Zn to 60 at % Zn. Anantharaman et.al. (26) studied the growth kinetics in an Al-28at%Zn alloy. A modified Turnbull model was used to study the kinetics of primary cellular reaction. It should also be noted that the choice of ageing temperatures was confined to the range 80°C to 150°C. Butler et.al. (27) investigated the cellular precipitation in Al-28 at % Zn alloy by making an insitu observation using high voltage electron microscope. They have observed that after nucleation at grain boundaries, the reaction proceeds at a linear growth rate. The modified model of Turnbull was used to study the growth kinetics. The variation of inter lamellar spacing with temperature of ageing was studied

and it was found that the value of inter lamellar spacing increased with increase in ageing temperature.

Malhotra and Rundman (25) studied the kinetics of discontinuous precipitation on Al-20 at%Zn alloy. The growth rate was evaluated from the transformed volume fraction data and the TTT curve was drawn. The effect of continuous precipitation on the discontinuous reaction was studied in the same alloy system.

Vijaylakshmi et.al. (29,30) have investigated the morphological features of the cellular precipitation in Al-Zn alloy system. They have reported the coarsening of the cellular precipitate at longer time of ageing.

Ju and Fournelle (4) have studied the morphology and kinetics of cellular decomposition and discontinuous coarsening in Al-29 at % Zn alloy. The kinetics of both Primary and secondary reactions were analysed using the model of Petermann and Hornbogen (7). Analysis of growth kinetics of both Primary and Secondary reactions indicated that the rate controlling mechanism is diffusion of solute through the grain boundary.

In this study we have investigated the kinetics of Primary reaction using the models of Cahn (8), Turnbull (9), Aaronson and Liu (10), Petermann and Hornbogen (7), Shapiro and Kirkaldy (12), and Sundquist (11). The Secondary reaction was analysed using the model of Petermann and

Hornbogen (7).

1.4 Models for Kinetics of Discontinuous Precipitation

1.4.1 Turnbull's Model for Growth Kinetics (9)

Consider the precipitation of β phase from a supersaturated solid solution α_o, forming in a lamellar morphology with the α phase. Following Zener's treatment of Pearlitic growth, the total flow of solute away from an a lamellae can be estimated by Fick's I-law

$$J = -D \frac{dc}{dx}$$

to give the rate of flow of atoms:

$$\frac{dm}{dt} = \frac{A^{\alpha} D}{V_M} \frac{dx_B}{dx} = \frac{A^{\alpha} D}{V_M} \frac{\Delta x_B}{L_{eff}} \qquad (1)$$

where,

A^{α} = area through which diffusion takes place

D = diffusion coefficient of the solute in the matrix

$\frac{\Delta x_B}{L_{eff}}$ = concentration gradient (L_{eff} = effective distance)

V_M = Molar volume.

Turnbull (9) considered a growth model for discontinuous precipitation based upon the diffusion of solute atoms through the grain boundary. The value of A^{α} in eqn.(1) will be equal to $b\,\delta$, where δ, is the boundary thickness and b is the distance parameter normal to the growth direction

and α/β interface. The effective distance, L_{eff}, is estimated to be equal to S^{α} and eqn.(1) becomes

$$\frac{dm}{dt} = \frac{b\,\delta D_b}{V_M} \cdot \frac{\Delta x_B}{S^{\alpha}} \qquad (2)$$

During discontinuous precipitation both α and β phases grow together as alternate lamellae. The width of the lamellae is related by Lever's principle as follows

$$\frac{S^{\alpha}}{V_M} = \frac{x_B^{\beta} - {}^{1}x_B^{\alpha}}{x_B^{\beta} - x_B^{\alpha}} \; \frac{S}{V_M} \quad \text{and} \quad \frac{S^{\beta}}{V_M} = \frac{{}^{1}x_B - x_B^{\alpha}}{x_B^{\beta} - x_B^{\alpha}} \; \frac{S}{V_M}$$

where,

x_B^{α} = mole fraction of component B in α phase

x_B^{β} = mole fraction of component B on β phase

${}^{1}x_B^{\alpha}$ = original alloy composition or mole fraction of component B in the supersaturated solid solution

S^{α} = width of the α lamellae

S^{β} = width of the β lamellae

V_M = molar volume

$$\frac{dm}{dt} = \frac{VbS^{\alpha}}{V_M}\left({}^{1}x_B^{\alpha} - x_B^{\alpha}\right) = \frac{VbS^{\beta}}{V_M}\left(x_B^{\beta} - {}^{1}x_B^{\alpha}\right) \qquad (3)$$

It is to be noted that in all models for cellular precipitation, the molar volumes of the phases present are assumed to be constant and equal to V_M.

Making the flux balance from Eqn.(2) and Eqn.(3),

$$\frac{VbS^{\alpha}}{V_M}\left({}^1x_B^{\alpha} - x_B^{\alpha}\right) = \frac{D_b\,\delta\,\Delta x_B}{S^{\alpha}}$$

or

$$V = \frac{D_b\,\delta\,\Delta x_B}{(S^{\alpha})^2\left({}^1x_B^{\alpha} - x_B^{\alpha}\right)} \tag{4}$$

where V denotes the growth velocity.

In approximating the concentration difference Δx_B, which drives the diffusion, Turnbull, neglected the effect of surface energy and used $\Delta x_B = {}^1x_B^{\alpha} - x_B^{\alpha/\beta}$ where $x_B^{\alpha/\beta}$ is the composition at the α/β interface. In addition he also neglected x_B^{α} in comparison to the original alloy composition ${}^1x_B^{\alpha}$ and thus was able to obtain the following equation for growth velocity

$$V = \frac{D_b\,\delta}{(S^{\alpha})^2} \cdot \frac{{}^1x_B^{\alpha} - x_B^{\alpha/\beta}}{{}^1x_B^{\alpha}} \tag{5}$$

1.4.2 Aaronson and Liu Treatment (10)

Aaronson and Liu (10) pointed out that in the growth velocity expression derived by Turnbull (9), x_B^{α} cannot be neglected in comparison with ${}^1x_B^{\alpha}$. By assuming $x_B^{\alpha} = x_B^{\alpha/\beta}$ and taking $A = 2b\,\delta$, since the material is leaving on both directions from the edge of the α lamellae and retaining the Zener approximation

$L_{eff} = \frac{S^{\alpha}}{2}$ they obtained an expression for the growth velocity

$$\frac{VbS^{\alpha}}{V_M}\left({}^{1}x_B^{\alpha} - x_B^{\alpha}\right) = \frac{2b\delta D_b}{V_M} \cdot \frac{{}^{1}x_B^{\alpha} - x_B^{\alpha/\beta}}{(S^{\alpha}/2)}$$

$$V = \frac{4\,D_b\delta}{S^2}\,\frac{(x_B^{\beta} - x_B^{\alpha})}{(x_B^{\beta} - {}^{1}x_B^{\alpha})} \qquad (6)$$

Here $L_{eff} = \frac{S}{2}$ and $S^{\alpha} = S\,\frac{(x_B^{\beta} - {}^{1}x_B^{\alpha})}{(x_B^{\beta} - x_B^{\alpha})}$

1.4.3 Cahn's Treatment (8)

It has been shown by Cahn (8) that the composition of the α lamellae in equilibrium with the β lamellae is not the equilibrium value. Due to the incomplete segregation of solute, only afraction of the total available free energy will be used to drive the reaction. A part of the available free energy $(P\Delta G_o + \frac{2\gamma V_M}{S})$ would be used as chemical free energy and the remaining $\frac{2\gamma V_M}{S}$ would be associated with the newly formed interface. In order to proceed with the problem it is necessary to assume that the reaction proceeds as fast as diffusion permits. It is also assumed that no diffusion occurs in the matrix except at the grain boundaries. The diffusion equation for cellular growth given by Cahn is,

$$D_b\,\delta\,\frac{d^2 x_B^b}{dy^2} + V({}^{1}x_B^{\alpha} - x_B^{\alpha}) = 0 \qquad (7)$$

where x_B^b is the composition at the boundary

y is distance along the boundary, measured normal to the lamellae.

Cahn also assumed that, $\frac{x_B^{\alpha}}{x_B^b} = k =$ constant, equilibrium exists at the α / β interfaces and that β lamellae are thin with respect to S (interlamellar spacing), so that the boundary conditions are:

$$x_B^{\alpha} = {}^{e}x_B^{\alpha} \quad \text{at} \quad y = \pm \frac{S}{2} \tag{8}$$

The solution to eqn.(7) is given by

$$\frac{x_B^{\alpha} - {}^{1}x_B^{\alpha}}{{}^{e}x_B^{\alpha} - {}^{1}x_B^{\alpha}} = \frac{\text{Cosh}\ (\frac{Z}{S}\sqrt{A})}{\text{Cosh}\ (\frac{1}{2}\sqrt{A})} \tag{9}$$

where,

$$A = \frac{K\ V\ S^2}{D_b\ \delta} \tag{10}$$

Cahn has approximated the chemical free energy change for non equilibrium segregation as,

$$\Delta F_c = -RT\ [{}^{1}x_B \ln \frac{{}^{1}x_B^{\alpha}}{{}^{e}x_B^{\alpha}} + {}^{1}x_A^{\alpha} \ln \frac{{}^{1}x_A^{\alpha}}{{}^{e}x_A^{\alpha}}]\ [1 - (\frac{x_B^{\alpha} - {}^{e}x_B^{\alpha}}{{}^{1}x_B^{\alpha} - {}^{e}x_B^{\alpha}})^2\ ] \tag{11}$$

The fraction P of the chemical free energy for equilibrium segregation actually released by cellular precipitation can be

obtained by integrating ΔF_c over the entire cell.

Substituting for x_B^α from eqn.(9) in equation (11) and integrating, we have

$$P = \frac{3}{\sqrt{A}} \tanh (1/2\sqrt{A}) - \frac{1}{2} \operatorname{sech}^2/(\sqrt{A}) \tag{12}$$

Cahn also evaluated the fraction of solute used during cellular precipitation as

$$W = \frac{2}{\sqrt{A}} \tanh \frac{\sqrt{A}}{2} \tag{13}$$

where W can be experimentally determined and hence A can be evaluated.

1.4.4 Petermann and Hornbogen's Treatment of Cellular Precipitation (7)

According to Petermann and Hornbogen (7), the growth velocity is given by,

$$V = -M \Delta G \tag{14}$$

where,

M = grain boundary mobility

ΔG = driving force for the growth of cells

The mobility is a function of temperature (T) and is determined from the atomic jump frequency $\frac{1}{\tau}$ (τ: period of jump) and the grain boundary thickness 'δ'. For the cell boundary to migrate, the solute atoms have to diffuse a distance equal to

$\frac{S}{2}$, to the β phase.

The time taken by the solute atom to move a distance $= \frac{S}{2}$ is given by

$$(\frac{S}{2})^2 = 2D_b \tau$$

Therefore,

$$\tau = \frac{S^2}{8D_b \delta} \qquad (15)$$

Substituting (15) in (24), we get,

$$V = - \frac{8D_b \delta}{RT\ S^2} \Delta G \qquad (16)$$

The amount of chemical free energy available to drive the reaction can be estimated with the help of free energy composition diagram.

$$\Delta G = P \Delta G_o + \frac{2\gamma V_M}{S} \qquad (17)$$

where,

γ = specific surface energy at the α/β interface

P = fraction of the chemical free energy, ΔG_o, released during the reaction

$$G = RT [{}^1x_B^\alpha \ln \frac{x_B^\alpha}{{}^1x_B^\alpha} + {}^1x_A^\alpha \ln \frac{x_A^\alpha}{{}^1x_A^\alpha}] + \frac{2\gamma V_M}{S} \qquad (18)$$

Considering equation (18), and equation (16), the equation for the growth velocity is as follows:

$$V = - \frac{8\ D_b \delta}{S^2\ RT} \{ [RT\ ({}^1x_B^\alpha \ln \frac{x_B^\alpha}{{}^1x_B} + {}^1x_A^\alpha \ln \frac{x_A^\alpha}{{}^1x_A})] + \frac{2\gamma V_M}{S} \} \quad (19)$$

1.4.5 Shapiro and Kirkaldy's Analysis (12)

Shapiro and Kirkaldy (12) suggested the existance of a metastable miscibility gap in the α solid solution. The reaction was then treated as an eutectoid reaction where there is a chemical driving force acting on the growth of the two lamellar phases. Following this they worked out the solution of the differential equation for the boundary conditions arising out of local equilibrium. The solution is as follows:

$$V_1\ S_1^3 = \frac{48\ D_b \delta\ V_M}{q(1/2 - {}^e x_B^\alpha)} \left(\frac{S_1}{S_c} - 1 \right) \quad (20)$$

where,

$$S_c = \frac{2\gamma V_M}{\Delta G_o} \quad (21)$$

The parameter 'q' is given by the expression

$$q = 1/2\ \frac{\partial^2 G^\alpha}{\partial x_B^{\alpha 2}} \quad \text{at} \quad {}^e x_B^\alpha \quad (22)$$

The value of q is determined from the equation:

$$\frac{\partial^2 G^\alpha}{\partial x_B^{\alpha 2}} = \frac{RT}{x_B^\alpha (1 - x_B^\alpha)} \quad (23)$$

1.4.6 Sundquist's Analysis (11)

Sundquist (11) wrote the diffusion equation (7) on the lines of Cahn (8) but instead of assuming a flat interface between α_o and α phases as done by Cahn (8), he solved the diffusion equation for a curved interface. The basic solution of the diffusion equation yields

$$\frac{x_B^{\alpha}(\bar{Z}) - {}^1x_B^{\alpha}}{x_B^{\alpha/\beta}(o) - {}^1x_B^{\alpha}} = \frac{\text{Cosh}\,(\sqrt{a} - (1 - \bar{Z}))}{\text{Cosh}\,\sqrt{a}} \tag{24}$$

where the parameter a is defined as

$$a = \frac{V_1\; S_1^2}{4D_b\delta K\,(\overline{\text{Cos}\theta})} \tag{25}$$

In eqn.(24), $x_B^{\alpha}(\bar{Z})$ is the average composition of the depleted matrix at position $\bar{Z}$ from the interface between α and β phases $x_B^{\alpha/\beta}(o)$ is the interface composition at the three phase function. Its value is very close to equilibrium solvus composition at the ageing temperature, but is formally defined by Sundquist to be related by

$$x_B^{\alpha/\beta}(o) = {}^e x_B^{\alpha/\beta} \exp \frac{2\; V_M\; \theta_o\; (x_B^{\beta} - x_B^{\alpha})}{RT\; S^{\alpha}\; W\; ({}^1x_B^{\alpha} - {}^e x_B^{\alpha/\beta})} \tag{26}$$

θ_o has a value of $\pi/6$. $\overline{\text{Cos}\theta}$, which is the average of the angle that the normal to the growth front makes with the growth direction is taken to be 0.7 as proposed by Sundquist (11)

The parameter a is determined from the relation

$$W = \frac{{}^{1}x_B^{\alpha} - x_B^{\alpha/\beta}(o)}{{}^{1}x_B^{\alpha} - {}^{e}x_B^{\alpha/\beta}} \quad \frac{\tan h \sqrt{a}}{\sqrt{a}} \tag{27}$$

1.4.7 Petermann and Hornbogen's Theory of Discontinuous Coarsening (7)

As shown earlier the growth velocity of the primary cells during cellular phase transformation is

$$V_1 = - \frac{8 D_b \delta}{RT\ S_1^2} \quad \Delta G_p \tag{28}$$

where ΔG_p is the chemical free energy ~~associated~~ used to drive the primary reaction

$$\Delta G_p = P\,\Delta G_o + \frac{2\gamma V_M}{S_1} \tag{29}$$

where,

$P\,\Delta G_o$ is the fraction of the total chemical free energy available to drive the primary reaction, a part of which $\frac{2\gamma V_M}{S_1}$ (+) goes to the newly created interface

$$V_1 = - \frac{8 D_b \delta}{RT\ S_1^2} \quad P\,\Delta G_o + \frac{2\gamma V_M}{S_1} \tag{30}$$

It is assumed that the remaining free energy is used in the growth of the secondary cells, then

$$\Delta G_2 = (1 - P)\,\Delta G_o \tag{31}$$

Using the above equations, the equation for secondary growth velocity, V_2 is given by

$$V_2 = - \frac{8\, D_b \delta}{S_2^2\, RT} \Delta G_s \tag{32}$$

where,

$$\Delta G_s = \Delta G_2 - \left(\frac{2\gamma\, V_M}{S_1} - \frac{2\gamma V_M}{S_2}\right) \tag{33}$$

CHAPTER 2

EXPERIMENTAL PROCEDURE

2.1 Alloy Preparation

The alloy for this investigation was prepared by using appropriate amounts of aluminum and zinc (both of 99.99% purity). Induction melting was carried out in a pure alumina crucible under argon atmosphere. The cast alloy was then hotrolled into strips of 2.5 mm thick. Thin foils of thickness 200 μ were also prepared for electron microscopy studies.

The samples for growth kinetics were prepared from the rolled strips. Samples 5mm x 5mm were cut and encapsulated in pyrex tubes after holding them under a vacuum of 10^{-3} torr or better for about 2-3 hours. Great care was taken to avoid any heating of the samples while sealing the capsules.

2.2 Heat Treatment of the Alloy

The samples were solution treated in **a tubular** furnace at 400°C ± 3°C for 36 hrs (to achieve a average grain size of 200 μ), and quenched in ice brine. The quenched samples were quickly transferred to a liquid N_2 bath in order to prevent the room temperature decomposition of the saturated solid solution.

The aging treatment for growth kinetics was done in a salt bath furnace for higher temperatures and in a oil bath for low temperatures. In each case the treatment was done after rigorous calibration of the bath. The temperature variation was found to be $\pm 1\,^{\circ}C$. The aged samples were quenched in ice brine and immediately taken for metallographic observation.

2.3 Examination of the Treated Specimens

The heat treated specimens were immediately mounted using a cold setting Resin and polished carefully for metallographic examination. The etchant used was Kellers Reagent (0.5% HF 1.5HCl 2.5% HNO_3).

2.3.1 Optical Microscopic Examination

The growth rate of the primary and secondary precipitates was found out by measuring the width of the grain boundary precipitate in a direction normal to the boundary. An average of 40 such measurements was taken to evaluate the growth rate by the principle of least squares.

2.3.2 Transmission Electron Microscope Examination

The thin foils which were heat treated with the bulk samples were cleaned and chemically thinned to 50 μ using 2.5% solution of HF in water. Electropolishing was done

by jet polishing technique. The electrolyte used was 10% perchloric acid and 90% methanol. The operating voltage was 15 volts DC and the temperature was maintained at 230°K.

The interlamellar spacing of the primary and secondary precipitates at each temperature was found out by counting the number of lamellae present in a specific distance. The average value was found out from 200 measurements.

2.4 X-ray Analysis

The composition of the depleted matrix, associated both with the primary and secondary reaction was determined by X-ray diffraction measurements carried out on the bulk samples. Cu K_{α} radiation was used with a Nickel filter. The value of Bragg angle was found out by measuring the angle of the

20} {420} and {331} peaks. The instrumentation correction was also incorporated in the calculation of the angle. This was done by measuring the Bragg angles of a standard silicon sample from the trace obtained at the end of the experiment.

The precise lattice parameter was evaluated and thereby the composition was calculated with the help of the data of Helfrich et.al.(32) for lattice parameter vs. composition on Al-Zn alloys.

CHAPTER 3

RESULTS AND DISCUSSION

3.1 Growth Rate

The growth rates of primary and secondary reactions were determined using optical microscopy. The width of the grain boundary precipitate was measured at different intervals of time for different temperature of ageing. In each case 50 different regions were observed and the width of the precipitate was measured in a normal direction to the boundary. The growth rates were then evaluated by least square method. The growth rates for Primary and Secondary reaction are presented in Table (1).

The growth rates of the Primary and Secondary reaction are found to be of the order of 10^{-8} M/sec and 10^{-10} M/sec respectively. The growth rate vs. temperature is shown in Fig.(2). It is clear from the plot, that growth velocity increases initially as the ageing temperature increases and reaches a maximum at 430°K. Thereafter with increase in temperature, it decreases. The nature of the secondary growth velocity is similar to the primary growth velocity. In this plot the data of Butler et.al. (26), Malhotra (25), Ju and Fournelle (4) are also indicated.

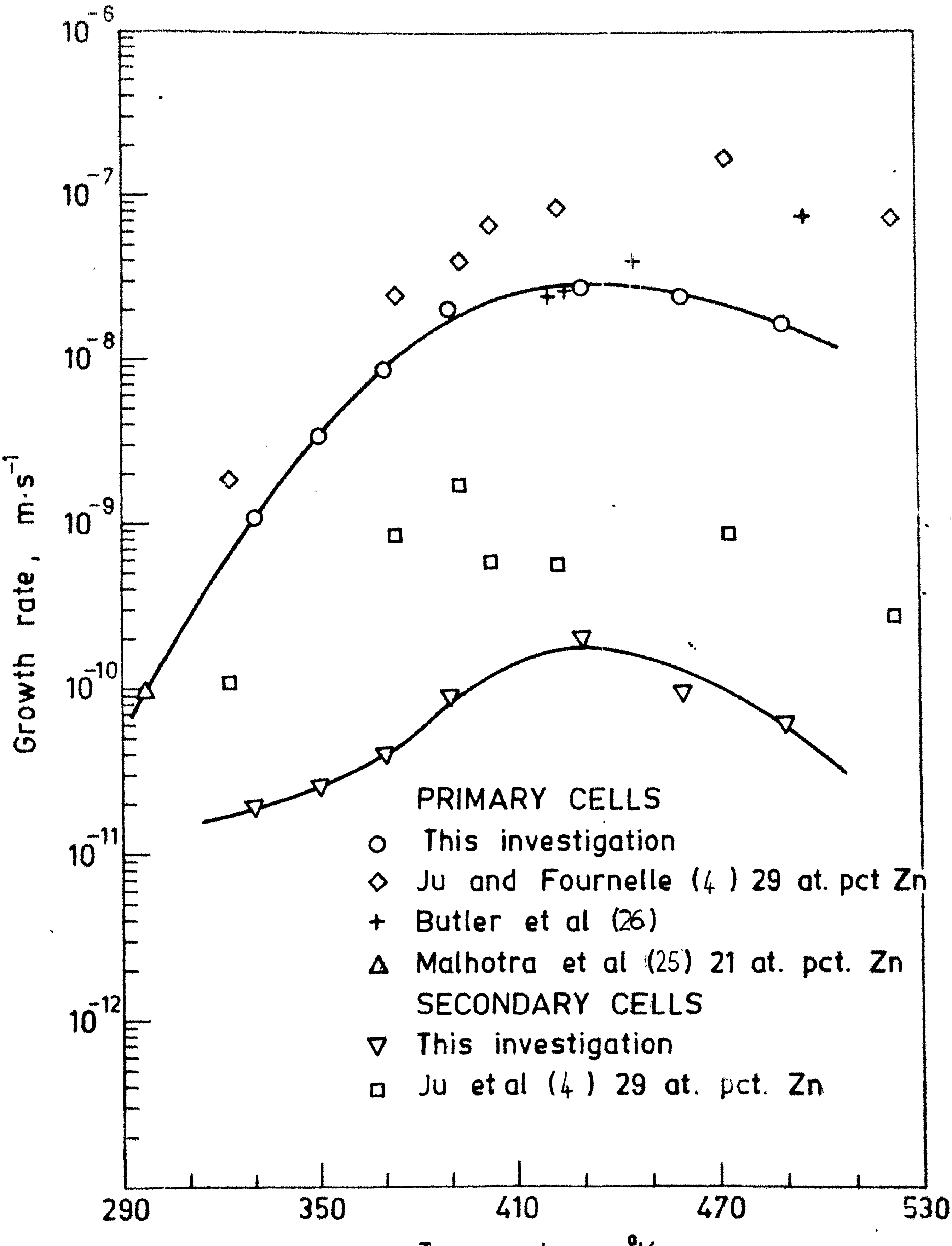

Fig. 2 Growth rate vs temperature.

The room temperature growth rate data of Malhotra (25) is also plotted in Fig.(2). The growth rate of the primary reaction in this study, when extrapolated to room temperature agrees with the value obtained by Malhotra for Al-22 at%Zn alloy. The growth rate of the primary reaction is found to have shape of a 'C' curve. This is also true with the data of Butler (26) and Ju, et.al. (4). However, it should be pointed out that the growth velocity values for primary reaction are lower because the original alloy composition was lower. This leads to a lower supersaturation and hence a lower value for the growth rate.

The growth rate of the secondary reaction is plotted against the temperature of ageing and is shown in Fig.(2). The growth rates of secondary reaction are 100 times lower ~~is~~ in magnitude than the primary reaction. The shape of the curve is like a 'C' curve with peak value of growth rate at 430°K. The growth rate of secondary reaction is dependent on the inter lamellar spacing and composition of α and β phases in a complex way (4). However it can be said that the low value for growth rate of the secondary reaction can be attributed to the smaller value of the driving force for the secondary reaction.

TABLE 1: Growth Rate, Interlamellar Spacing and Composition Data of Primary and Secondary Cell Growth

T °K	V_1 x $10^8 MS^{-1}$	S_1 x $10^7 M$	$P_{X_B}^{\alpha}$	V_2 x $10^{10} MS^{-1}$	S_2 x$10^7 M$	$S_{X_B}^{\alpha}$	X_B^{β}
490	1.665	4.65	0.060	0.616	16.57	0.060	0.9903
460	2.236	3.28	0.069	0.959	11.52	0.0453	0.9932
430	2.470	2.38	0.079	1.82	7.9	0.033	0.9951
390	2.00	1.72	0.08325	0.831	7.2	0.0252	0.9966
370	0.829	1.52	0.0857	0.386	5.86	0.0236	0.9977
350	0.326	1.37	0.850	0.233	4.71	0.02336	0.9982
330	0.110	1.37	0.084	0.18	3.65	0.02566	0.9985

3.2 Interlamellar Spacing

The interlamellar spacings for the Primary and Secondary reaction measured at different temperatures are shown in Table (1). The primary and secondary cells have an interlamellar spacing whose magnitude is in the range of 10^{-7} metres. The primary and secondary cell interlamellar spacings were measured using Transmission Electron Microscope. Thin foils treated along with the bulk specimens were used for this study. For each temperature an average of 200 readings was taken to evaluate the interlamellar spacing. A plot of interlamellar spacing against temperature is shown in Fig.(3). It is seen that the interlamellar spacing increases steadily with increase in ageing temperature. This behaviour has been observed in other studies too (4,31). It is seen that the values of interlamellar spacing obtained for primary reaction in this study are higher than those values reported in earlier studies. The reason for this, is the composition of the original alloy. In this case, the study was carried out on Al-20 at%Zn alloy, which is lower than the composition used in other studies (29 at%Zn). As seen earlier the growth rate is slower in this case and this enables the solute to traverse larger distances.

The interlamellar spacings of the secondary cells are 4 times larger in magnitude than the primary cells

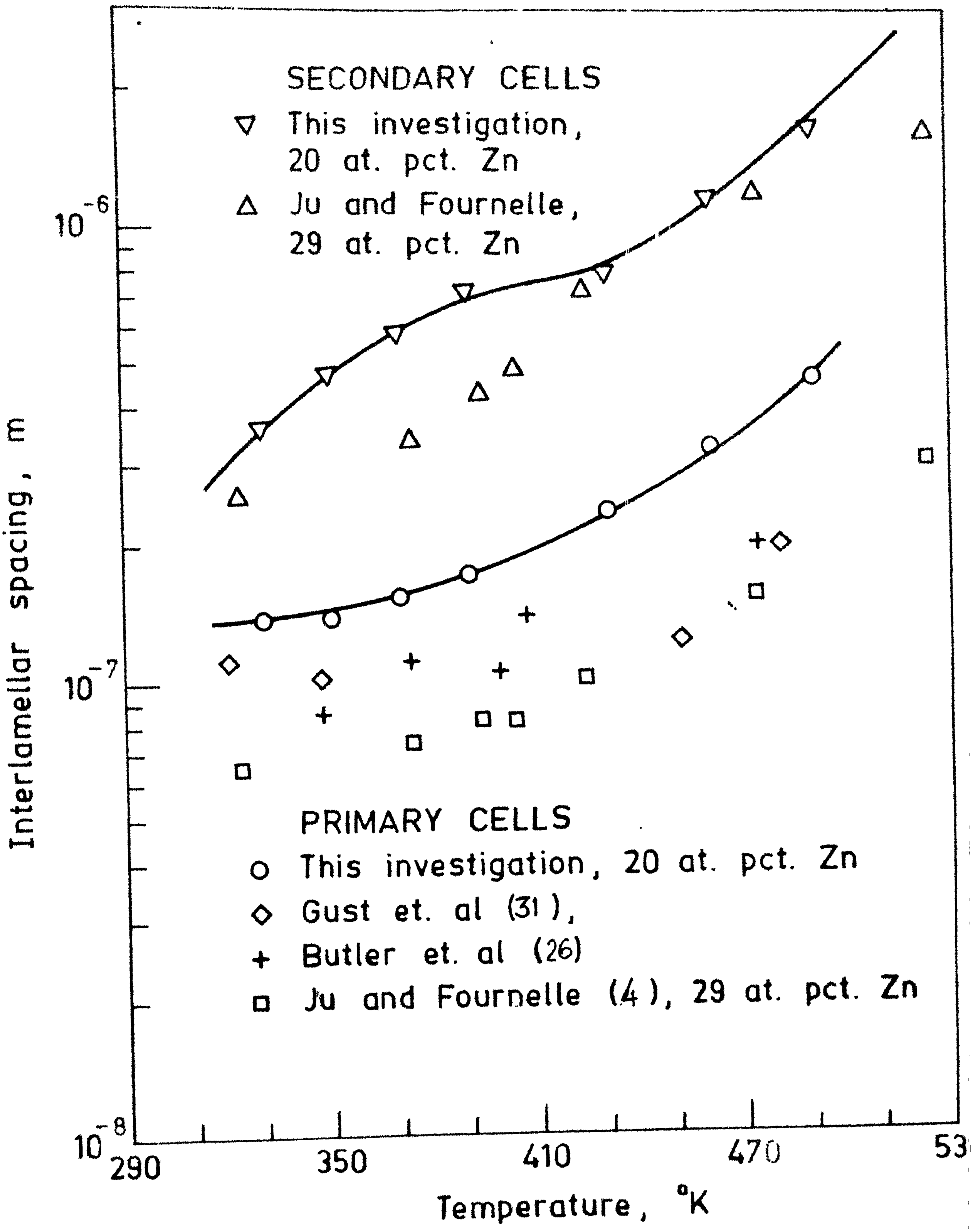

Fig. 3 Interlamellar spacing vs temperature.

The value of cell spacing in^reases with increase in ageing temperature as is evident from the Fig.(3). The slower growth rate is responsible for larger value of inter-lamellar spacing. A plot of interlamellar spacing against ΔT was plotted to find out the relationship between the two parameters. This is shown in Fig.4. It is seen that the graph is straight line with slope equal to -1.04 and -1.05 for the Primary and Secondary cells respectively. It can be concluded that S varies inversely as ΔT and this has been found true in many other alloy systems (2,3)

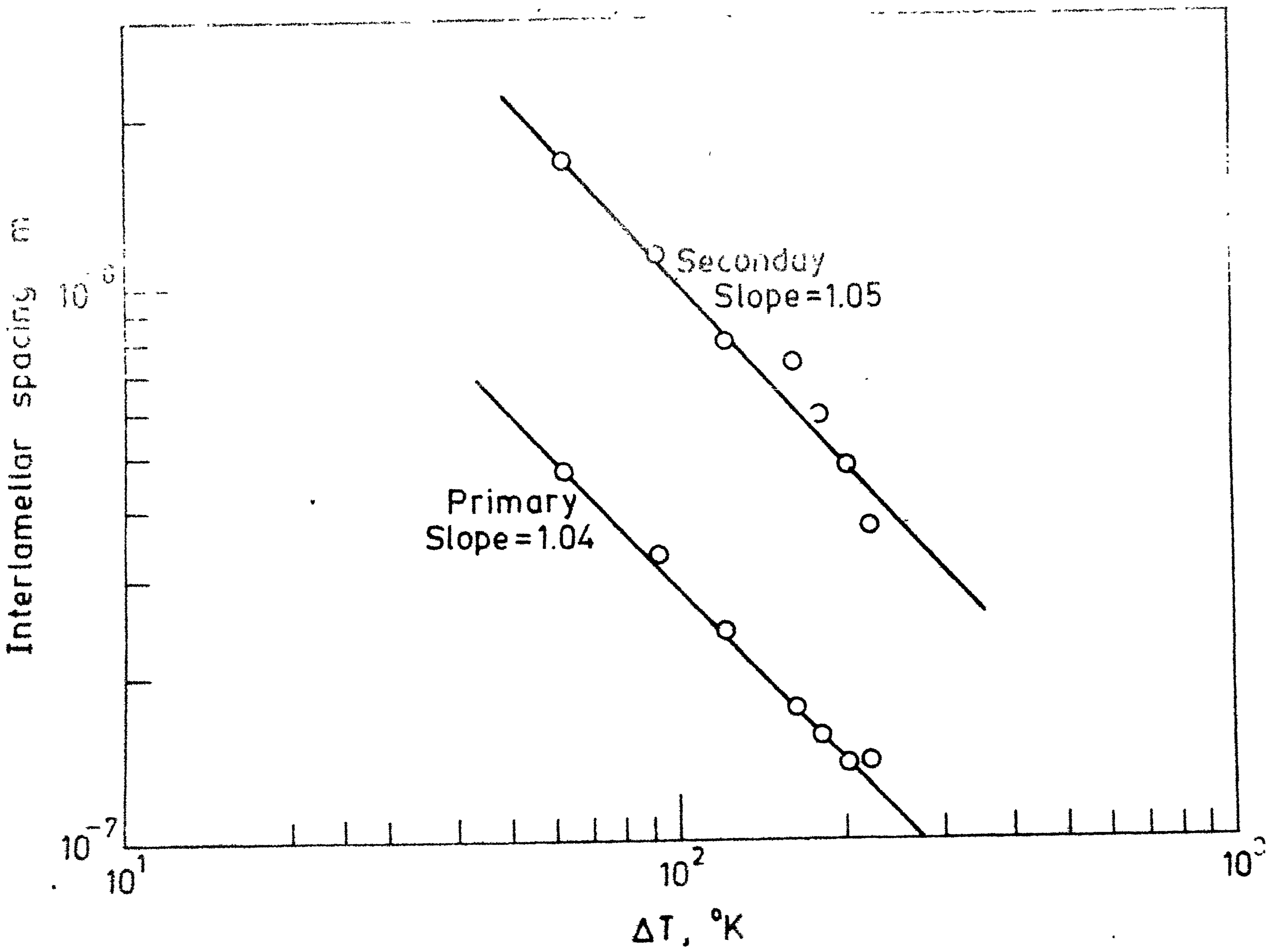

Fig.4 Interlamellar spacing vs ΔT.

3.3 Composition of the Depleted Matrix

The composition of the depleted matrix for Primary and Secondary reaction were determined by x-ray diffraction technique. The composition was determined by measuring the value of Bragg angle (2θ) at the peak positions of the {420} and {331} diffraction peaks. The specimens used for this measurement had been checked by optical microscope to ensure that microstructure had fully transformed structure of primary cells or predominantly secondary cells, as was the case. The lattice parameter was evaluated directly, as there was no overlapping of peaks. The composition of the α -phase was evaluated from the lattice parameter-composition data of Helfrich and Dodd (32) as shown in Fig.(5).

The composition of the depleted matrix of the primary and secondary reaction is plotted against the temperature as shown in Fig.(6). The solvus line of the Al-Zn equilibrium diagram (36) is also shown. It is seen that the solvus curve for the primary reaction is far away to the right of the equilibrium, solvus, except at the highest temperature, 490°K. Ju and Fournelle (4) also determined the composition of the α phase for the Primary reaction in Al-29 at% Zn alloy. The shape of the solvus is identical to that obtained in this study. It was observed that the composition values were higher in the study of Ju and Fournelle (4). This

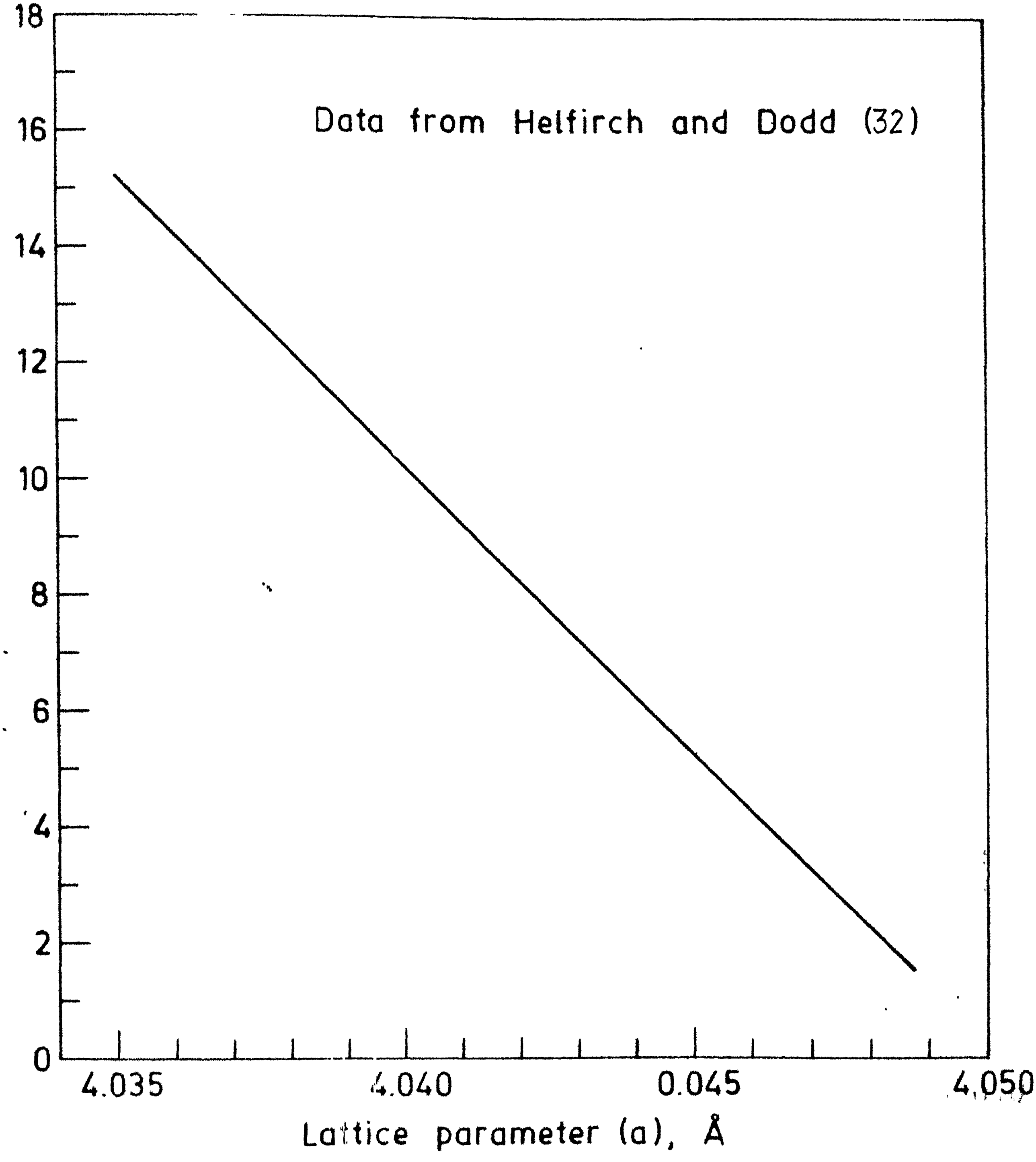

Fig.5 Lattice parameter vs composition.

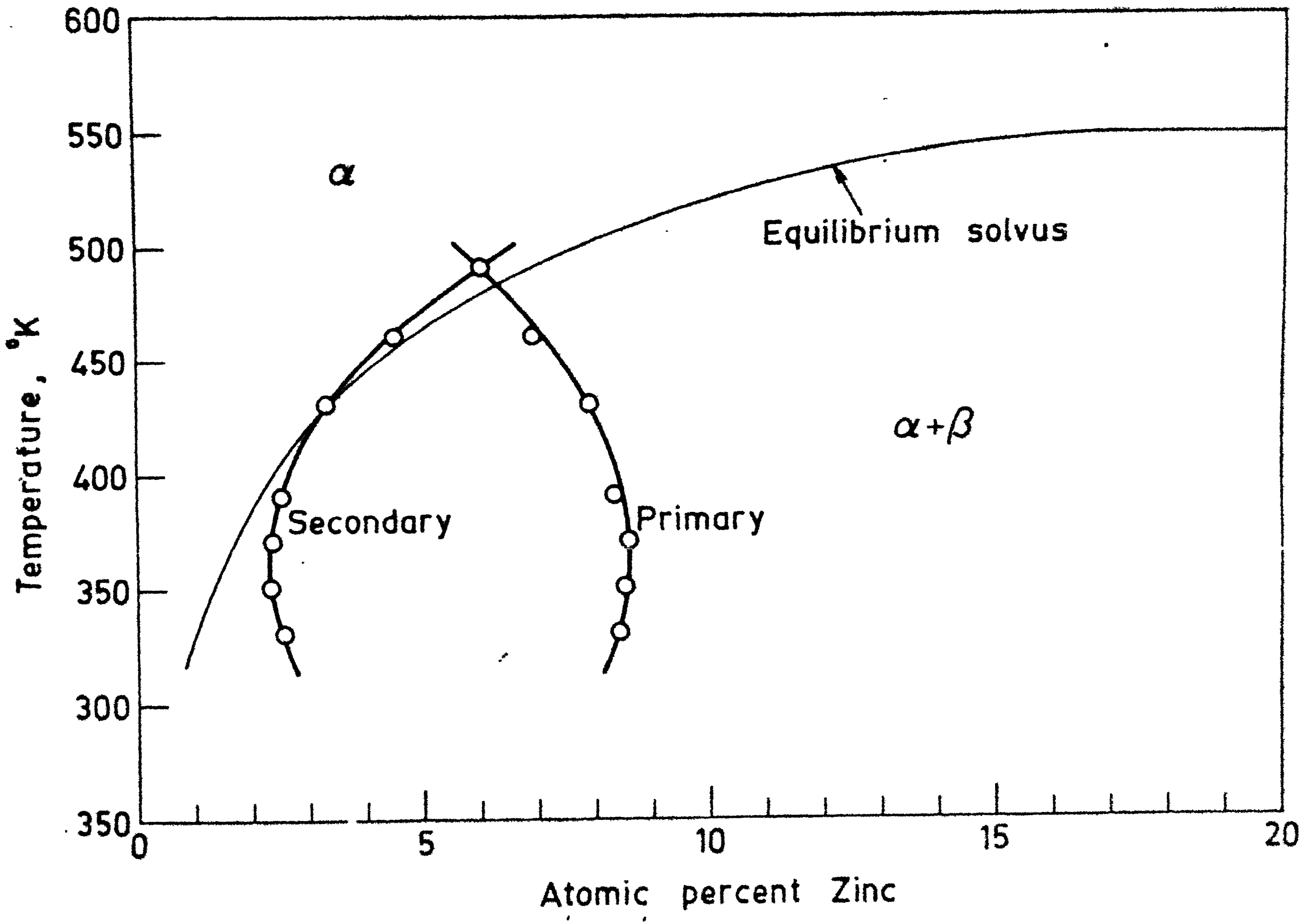
600
550
500
450
400
350
300
350
0
5
10
15
20
Temperature, °K
Atomic percent Zinc
α
α+β
Equilibrium solvus
Secondary
Primary

is because of the increased supersaturation and higher growth velocity and by Cahn's explanation that increased supersaturation causes a shift towards a higher composition for the α phase. The general precipitation within the lamellae is not observed in this study as was observed by Ju and Fournelle (4). The reason for this is because the supersaturation is lower by about 10 at% in this study and the corresponding α phase composition was lower. The composition of the depleted matrix for primary and secondary reaction is presented in Table (1).

The α phase composition of the secondary reaction was determined in a similar way as that of the Primary reaction. It is obvious that the composition of the depleted matrix of the secondary reaction is lower than the primary reaction as the reaction proceeds towards equilibrium. The value of X_B^α at the highest temperature falls outside the equilibrium solvus. This is not possible, however, it could happen as the composition is calculated from the reported lattice parameter vs. composite data. Ju et.al. (4) also had similar problem and they attributed the situation due to error in the lattice parameter composition relationship or the aluminum - zinc equilibrium phase diagram.

3.4 Calculation of Driving Force for Cellular Precipitation

The driving force for both primary and secondary reaction was evaluated from the basic thermodynamic equation.

$$\Delta \overline{G^M} = \Delta \overline{H^M} - T \Delta \overline{S^M} \tag{34}$$

where $\Delta \overline{H^M}$ and $\Delta \overline{S^M}$ are the changes in partial molar enthalpy and entropy respectively. The values of $\Delta \overline{H^M}$ and $\Delta \overline{S^M}$ for this alloy composition were taken from the data published by Hilliard et.al. (33). It was assumed that the relative partial molal enthalpy and entropy of Zn in the α phase are constant. Figure (7) shows the variation of enthalpy and entropy values at 573°K. The absolute values were obtained by multiplying with the appropriate composition of the α phase. It was also assumed that the β phase had a composition close to pure zinc from the phase diagram.

The variation of the overall free energy ΔG, is plotted against temperature in Fig.(8). It is seen that at 490°K the value of ΔG_0 and ΔG_1 are equal. As the temperature of ageing is decreased ΔG_0 decreases (becomes more negative) in magnitude, which is consistent with the concept that ΔG_0 varies inversely with the degree of undercooling. The values of the free energy change for primary and secondary reaction are evaluated. Representation plots of the free energy composition diagram are shown in Fig. 9 and

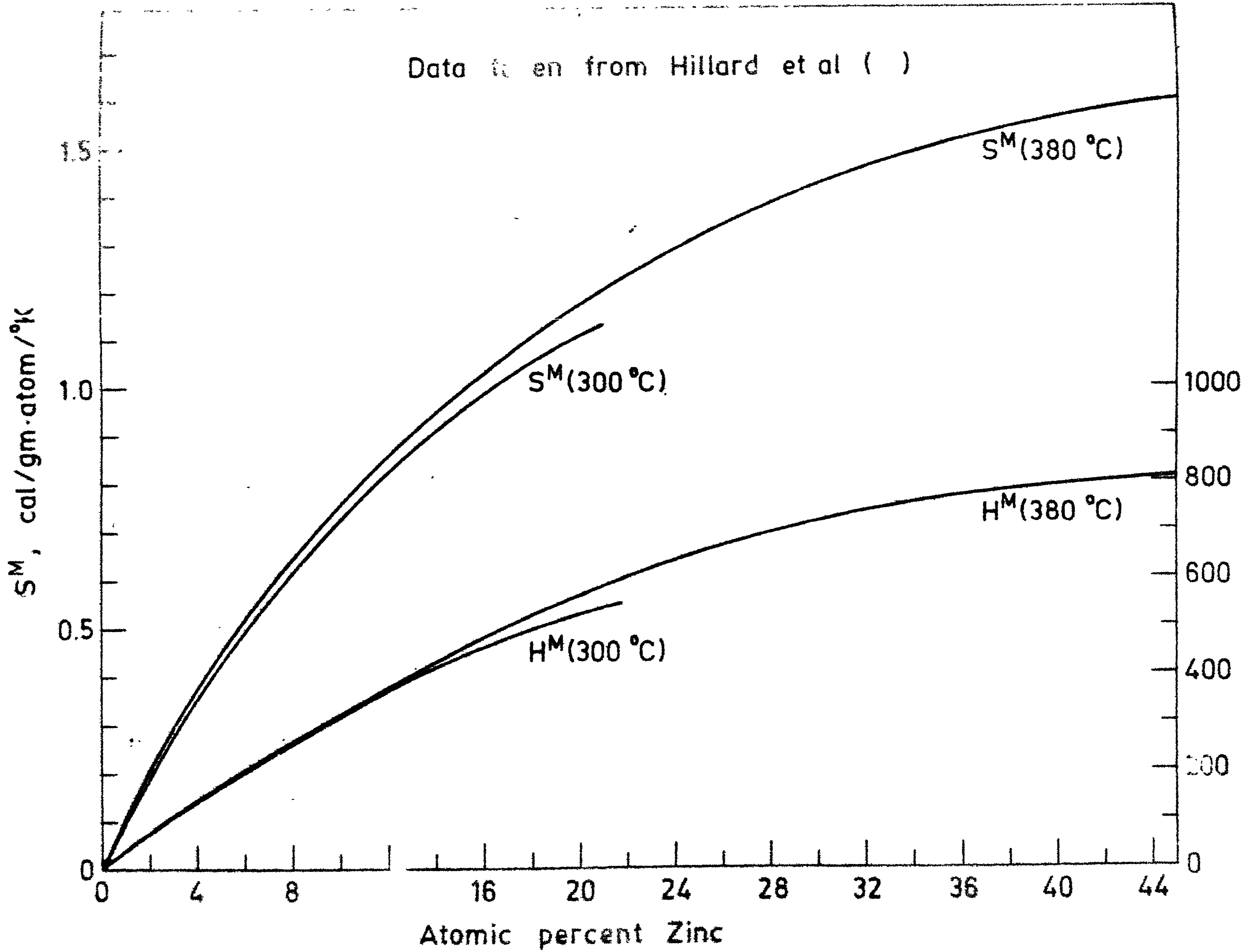

Data t en from Hillard et al ( )
S^M(380 °C)
S^M(300 °C)
H^M(380 °C)
H^M(300 °C)
S^M, cal/gm·atom/°K
H^M, cal/mole
Atomic percent Zinc
0
0.5
1.0
1.5
0
400
600
800
1000
0
4
8
16
20
24
28
32
36
40
44

Fig 7

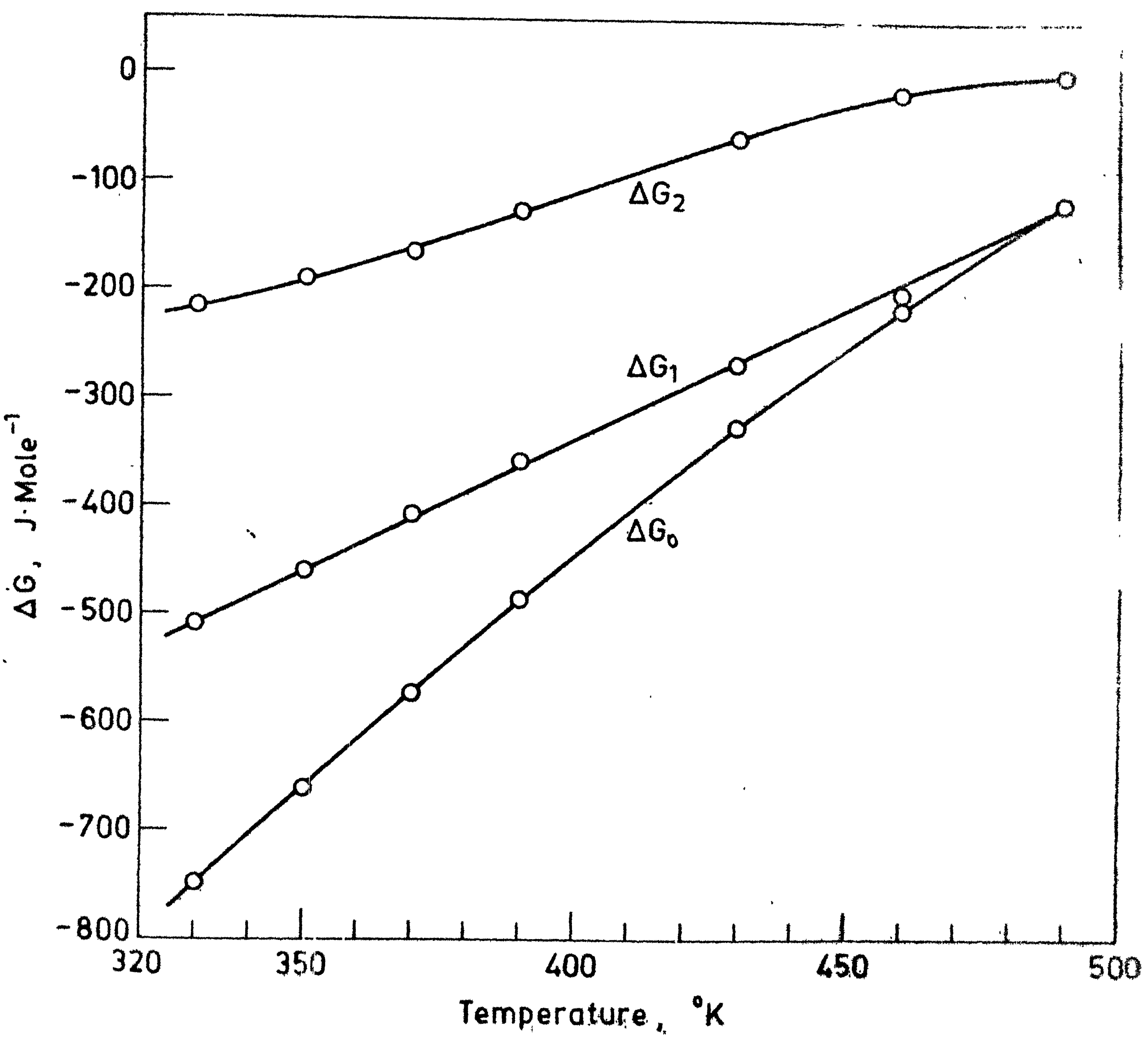

0
-100
-200
-300
-400
-500
-600
-700
-800
ΔG, J·Mole^{-1}
320
350
400
450
500
Temperature, °K
ΔG_2
ΔG_1
ΔG_0

Fig. 8

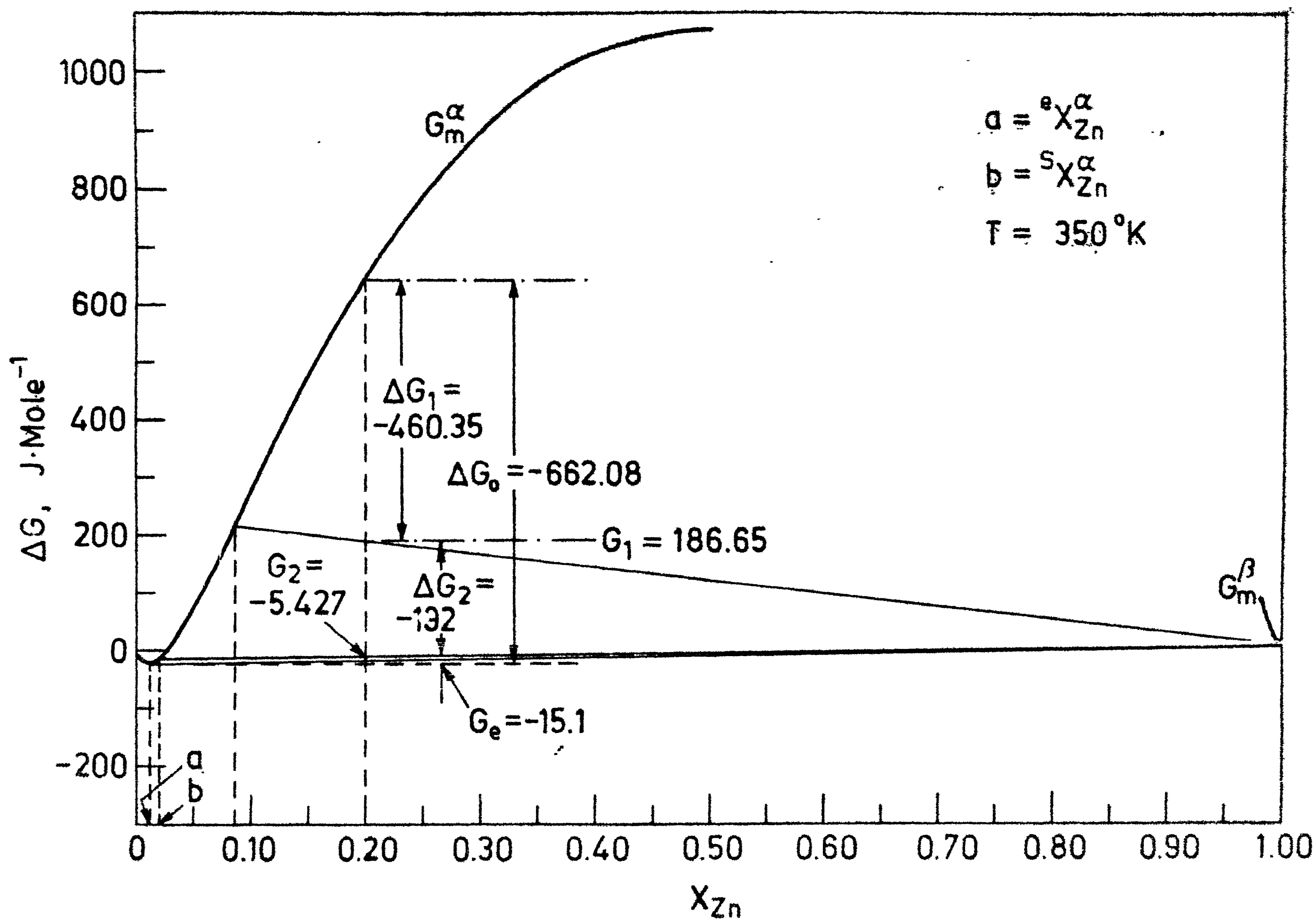

1000
800
600
400
200
0
-200
ΔG, J·Mole⁻¹
0
0.10
0.20
0.30
0.40
0.50
0.60
0.70
0.80
0.90
1.00
X_{Zn}
G_m^{α}
G_m^{β}
$a = {}^{e}X_{Zn}^{\alpha}$
$b = {}^{s}X_{Zn}^{\alpha}$
$T = 350\,^{\circ}K$
$\Delta G_1 = -460.35$
$\Delta G_o = -662.08$
$G_1 = 186.65$
$G_2 = -5.427$
$\Delta G_2 = -132$
$G_e = -15.1$
a
b

Fig. 9

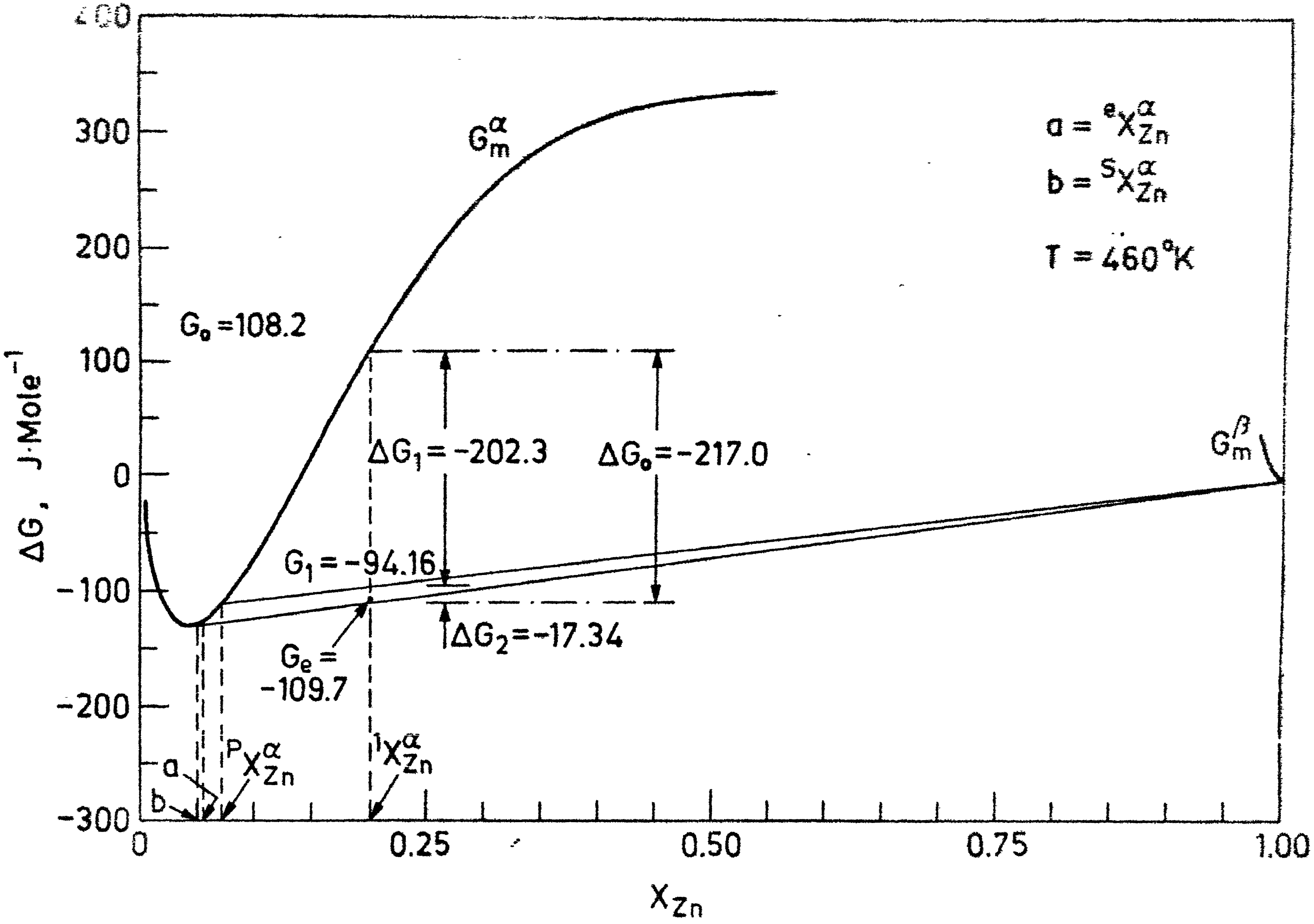

ΔG, J·Mole⁻¹
400
300
200
100
0
−100
−200
−300
0
0.25
0.50
0.75
1.00
X_Zn
G_m^α
G_m^β
$a = {}^eX_{Zn}^\alpha$
$b = {}^sX_{Zn}^\alpha$
$T = 460°K$
$G_o = 108.2$
$\Delta G_1 = -202.3$
$\Delta G_o = -217.0$
$G_1 = -94.16$
$\Delta G_2 = -17.34$
$G_e =$
-109.7
a
b
${}^PX_{Zn}^\alpha$
${}^1X_{Zn}^\alpha$

Fig. 10

Fig.10. The values of ΔG_p and ΔG_s are evaluated from Fig.9 and Fig.10. ΔG_p is the chemical free energy associated with the primary reaction and ΔG_s is the chemical free energy associated with the secondary reaction.

The surface energy γ, was calculated using equation

$$\gamma = H_\gamma - TS_\gamma \tag{35}$$

The enthalpy, H_γ and entropy S_γ values were taken from the work of Cheetham and Sale (35) on lamellar Al-Zn eutectoids. The values are shown in Table 2.

The driving force for the primary cellular reaction, ΔG_p is evaluated by deducting the surface energy from the chemical free energy available for primary precipitation. Similar calculation is made for the secondary reaction.

$$\Delta G_p' = \Delta G_1 + \frac{2\gamma V_M}{S_1} \tag{36}$$

$$\Delta G_s = \Delta G_2 - \left(\frac{2\gamma V_M}{S_1} - \frac{2\gamma V_M}{S_2}\right) \tag{37}$$

The chemical free energy and surface free energy associated with primary and secondary reaction are also given in Table (2). The values of various free energy terms are given in Table (3).

TABLE 2 : Chemical Free Energy and Surface Free Energy Associated with Primary and Secondary Cellular Reaction*

$$V_M = 9.855\text{x}10^{-6} M^3 \text{mole}^{-1}$$

T°K	γ (J/M^2)	$\frac{2\gamma V_M}{S_1}$ (J/mole)	$\Delta G_p = \Delta G_1 + \frac{2\gamma V_M}{S_1}$ (J/mole)	$\frac{2\gamma V_M}{S_2}$ (J/mole)	$\Delta G_s = \Delta G_2 - (\frac{2\gamma V_M}{S_1} - \frac{2\gamma V_M}{S_2})$ (J/mole)	$(\frac{2\gamma V_M}{S_1} - \frac{2\gamma V_M}{S_2})$ (J/mole)
490	0.3966	16.8	-101.9	4.71	-12.1	+ 12.10
460	0.4164	25.0	-177.3	7.12	-35.22	+ 17.88
430	0.4362	36.0	-232.5	10.88	-85.92	+ 25.12
390	0.4626	52.95	-305.55	12.62	-168.93	+ 40.30
370	0.4758	61.41	-344.58	16.00	-210.00	+ 45.41
350	0.5022	72.00	-437.40	27.10	-262.50	44.90

*Calculated from the thermodynamic data of Hilliard et.al. (33) and Cheetham and Sale (35).

TABLE 3 : Free Energy Values Calculated from the Data of Hilliard et.al. (33)

T°K	G_o J mole^{-1}	G_1 J mole^{-1}	ΔG_1 J mole^{-1}	G_2 J mole^{-1}	ΔG_2 J mole^{-1}	G_e^{α} J mole^{-1}	ΔG_o J mole^{-1}
490	-38.8	-157.4	-118.7	-157.5	0	-180.74	-118.03
460	+108.2	- 94.16	-202.3	-111.5	17.34	-130.5	-217.35
430	255.15	- 13.4	-268.5	- 74.2	-60.8	- 88	-326.95
390	451.1	+ 92.4	-358.6	- 36.2	-128.6	- 47.5	-487.7
370	549.1	143.3	-406	-21.26	-164.56	- 33.77	-574.62
350	647	186.6	-460.3	-5.427	-192	- 20.9	-662
330	745	235.6	-509.4	+18	-217.6	- 8.11	-749

3.5 Kinetics of Primary Cellular Reaction

The kinetics of primary cellular reaction was analysed using models proposed by Turnbull (9), Aaronson and Liu (10), Cahn (8), Petermann and Hornbogen (7), Shapiro and Kirkaldy (12) and Sundquist (11). For each of the models the Arrhenius plot of ln D_b against (1/T) was plotted. The plots are shown in Figs.(11) and (12). The activation energy for the primary cellular reaction was evaluated. It is observed that the models of Cahn (8), Petermann and Hornbogen (7) and Sundquist (11) yield a higher value of activation energy than the other models. The value of 60 kJmole^{-1} observed for the three models falls in the range of 1/2 to 2/3 of the activation energy for volume diffusion (Q_v = 104 kJmole^{-1}) reported by Hilliard ét.al.(34) from inter diffusion studies of zinc and aluminum. In the case of other models (Turnbull, Aaronson, Kirkaldy), the value of activation energy is about 48 kJmole^{-1}. In other studies of cellular precipitation on the Cahn's model always yields a lower value of activation energy. However in this case the higher value of activation energy can be attributed to the shape of the solvus curve for the primary reaction which shows a decrease in zinc concentration as the temperature increases.

The volume diffusion coefficient, D_v, was calculated by assuming the value of D_o (D_o = 1.0x10^{-5}M^2/sec) and

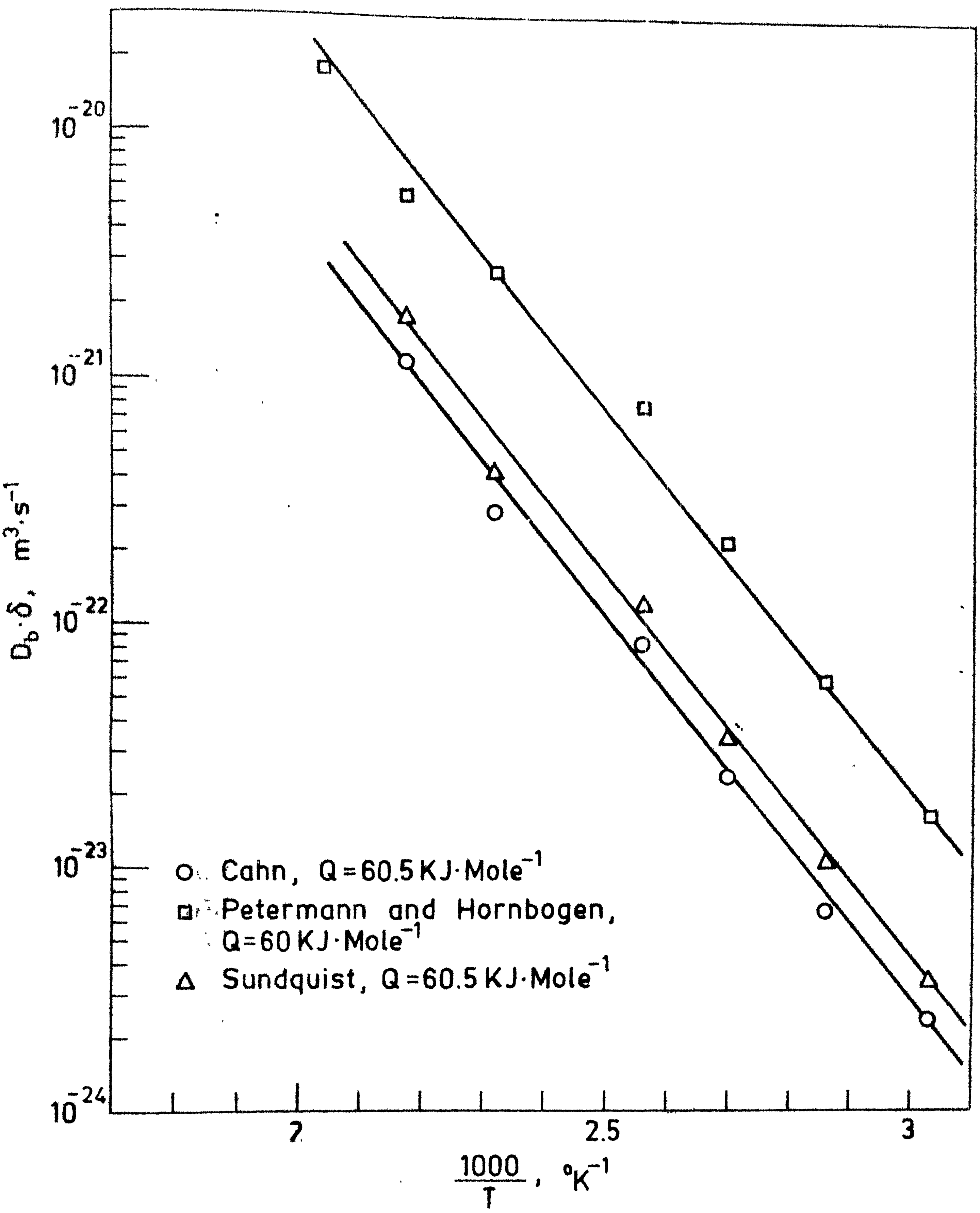

Fig. 11 $D_b \cdot \delta$ vs $\frac{1}{T}$.

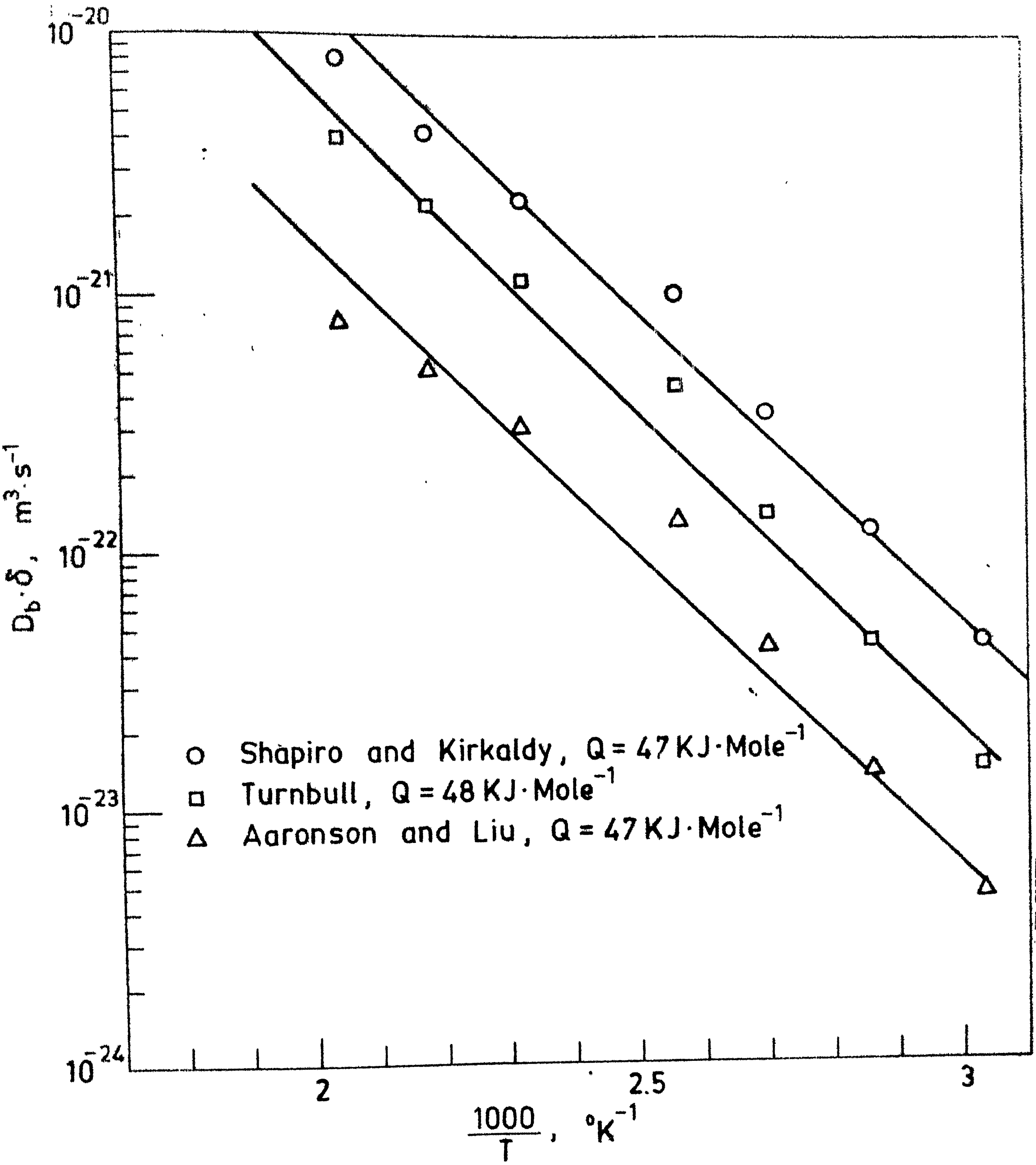

Fig. 12 $D_b \cdot \delta$ vs $\frac{1}{T}$.

Q_v = 104 kJ mole^{-1} from the published data of Hilliard et.al. (34). The values of D_v and $D_v \delta$ are found out and are shown in Table (5). It is observed that at lower ageing temperatures the values of $D_v \delta$ are much lower than the $D_b \delta$ values. At 490°K the value of $D_v \delta$ is 3.62×10^{-26} M^3/sec.

The effective diffusion time for the primary reaction can be calculated using the equation, $\bar{x} = \sqrt{Dt}$ where $\bar{x}$ is the effective diffusion distance which can be taken to be equal to the interlamellar spacing and D is the volume diffusivity of zinc calculated by assuming $D_o = 1.0 \times 10^{-5}$ M^2/sec and Q = 104 kJ mole^{-1}. The value of time obtained by taking D_v into consideration is about 500 times higher than the observed time for completion of the primary reaction. This gives sufficient reason for us to conclude that the cellular reaction in Al-Zn alloy system is controlled by grain boundary diffusion. This has also been found true in other systems exhibiting cellular reaction (1,2,3). In the analysis of growth kinetics it has been assumed that the general precipitation has negligible effect on the cellular growth. This has also been pointed out by Ju and Fournelle (4) in his study on Al-29 at%Zn alloy. They determined the magnitude of this effect in the analysis of Petermann and Hornbogen (7). It was reported that the driving force for the primary reaction reduced by 15% and thereby yielded a higher value of $D_b \delta$. The values of

$D_b\,\delta$ are presented in Table 4 for all the models. The activation energy for boundary diffusion, Q and the diffusivity values of D_b at 400°K are presented in Table 5. The Table also shows the volume diffusivity values for comparison. The pre exponential constant, D_b^o is calculated for various models at 400°K from the equation

$$D_b = D_b^o \exp(-Q/RT) \qquad (38)$$

D_b = boundary diffusivity of zinc

Q = activation energy for boundary diffusion

T = 400°K

R = 8.314 J/°K/mole.

The individual values of D_b^o are listed in Table (5). It is seen that the $D_b o$ values for each model falls in the same order of magnitude except the value of D_b^o of the Aaronson and Liu (10) model. The value of D_b^o depends on the value of Q which is inturn dependent on the ΔG value.

One of the reasons for the success of Petermann and Hornbogen model is that at higher temperatures the value of the driving force is smaller and this yields a higher value of $D_b\,\delta$. This results into a higher Q value, although the data fits better in the whole range of temperature.

TABLE 4 : $D_b\delta$ Values for Primary and Secondary Cell Growth

T	Cahn $x10^{22} M^3 S^{-1}$	Petermann and Hornbogen $x10^{22} M^3 S^{-1}$	Shapiro and Kirkaldy $x10^{22} M^3 S^{-1}$	Turnbulle $x10^{22} M^3 S^{-1}$	Aaronson & Liu $x10^{22} M^3 S^{-1}$	Sundquist $x10^{22} M^3 S^{-1}$	Petermann & Hornbogen (Secondary $x10^{22} M^3 S^{-1}$
490	-	180	80.3	40.44	7.646	-	71.18
460	11.6	65	41.9	22.11	5.166	17.6	17.3
430	2.858	27	23.0	11.52	3.056	4.22	5.9
390	0.825	7.8	10.18	4.4	1.293	1.21	1.04
370	0.235	2.157	3.42	1.4	0.422	0.339	0.243
350	0.668	0.57	1.18	0.437	0.136	0.106	0.0782
330	0.0239	0.16	0.435	0.143	0.0454	0.0347	0.0314

Table 5 : Activation Energy, Diffusivity and D_o Values for Different Theories; Volume Diffusion Data obtained from the Data of Hilliard et.al. (34) is also shown for comparison

Theory	Activation energy Q kJ/mole	$D_b\delta$ (at 400°K) x $10^{22} M^3 S^{-1}$	D_b(400°K) $10^{22} M^2 S^{-1}$	$D_b o$ x$10^5 M^2 S^{-1}$	D_v (400°K) x $10^{19} M^2 S^{-1}$
Cahn	60.5	1.1	0.22	1.7506	2.25
Turnbull	48	3.5	0.7	12.98	2.25
Aaronson & Liu	47	1.0	0.2	0.0274	2.25
Sundquist	60.5	1.7	0.34	2.705	2.25
Shapiro & Kirkaldy	47	8.5	1.7	23.347	2.25
Petermann & Hornbogen (Primary)	60	7.8	1.56	10.68	2.25
Petermann & Hornbogen (Secondary)	61	1.55	0.33	3.652	2.23

3.6 Kinetics of Discontinuous Coarsening: Secondary Reaction

The kinetics of discontinuous coarsening of the cellular reaction was analysed using the model of Petermann and Hornbogen (7). Accordingly the rate of growth of secondary cell is given by

$$V_2 = \frac{8\, D_b \delta}{RT\, S_2^2} \Delta G_s \qquad (39)$$

where ΔG_s - driving force used for the secondary reaction. A plot of ln $D_b\ \delta$ against (1/T) is shown in Fig.(13). In the analysis of Petermann and Hornbogen (7) it is assumed that the remaining free energy after the primary reaction drives the secondary reaction. The value of activation energy obtained for the secondary reaction is about 61 kJ mole^{-1}. The free energy is further reduced during the secondary reaction by decreasing the interfacial energy. The decrease in total free energy of the coarsened or secondary precipitate has two terms: (i) free energy change arising only from changes in composition of the phases, termed as the 'chemical free energy change' and (ii) the change in interfacial energy due to coarsening. The amount of interfacial energy released and used as a part of the chemical free energy required in the secondary reaction is given by $\left(\frac{2\gamma V_M}{S_2} - \frac{2\gamma V_M}{S_1}\right)$, according to Fournelle (1). These values are also listed in Table (5).

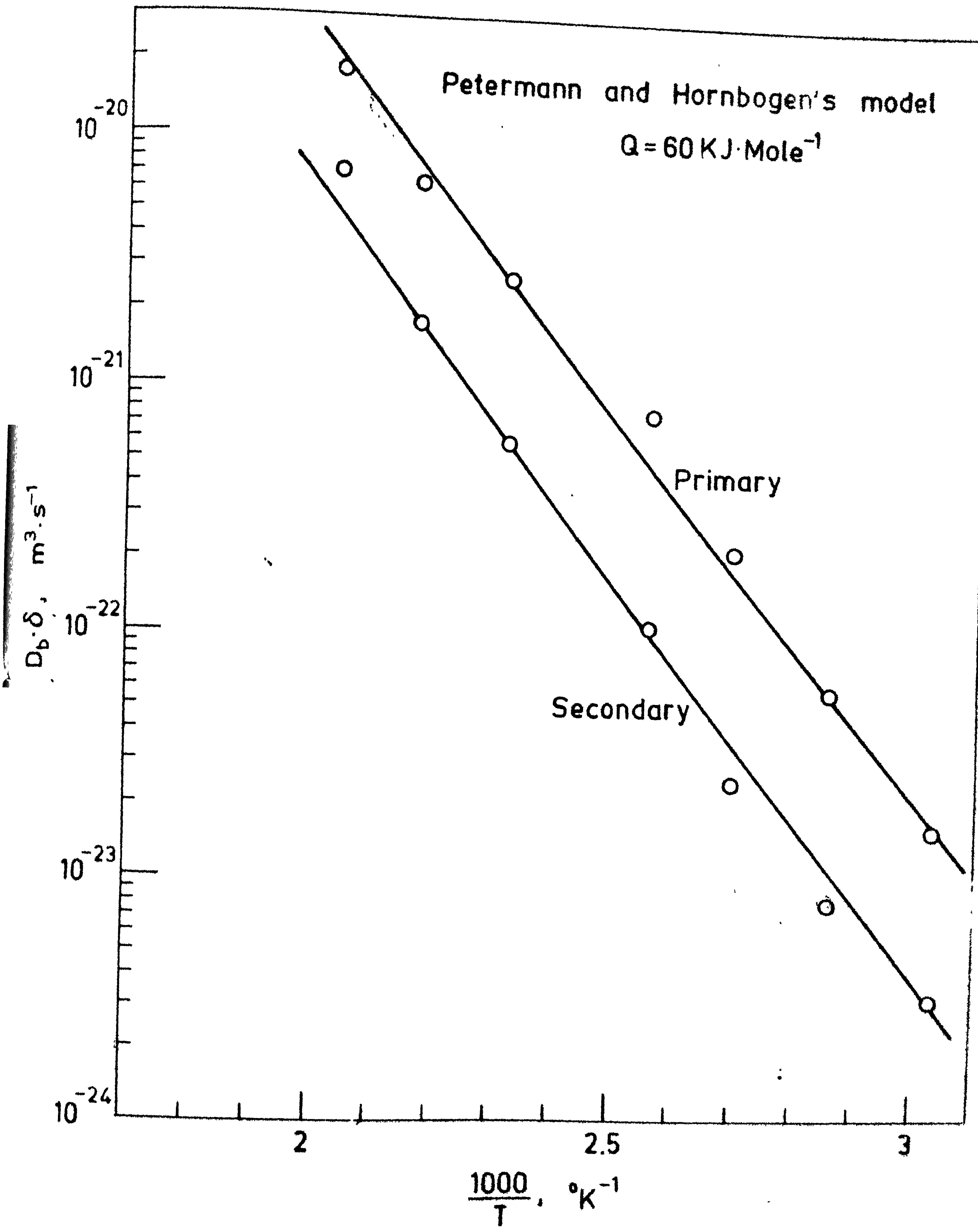

Fig. 13 $D_b \cdot \delta$ vs $\frac{1}{T}$.

It is observed that the interfacial energies of both precipitates increase with a decrease in the temperature of ageing. The values range from 16.8 J/mole to 72 J/mole for primary and 4.71 J/mole to 27.1 J/mole for the secondary. The results obtained support the fact that the interfacial energy decreases as the coarsening proceeds.

The secondary reaction involves two processes:

(i) dissolution of the primary ahead of the reaction front and

(ii) redistribution of the solute atoms at the reaction front.

During the coarsening a part of the driving force is released at the primary secondary reaction front. The interlamellar spacing of the secondary cell are the deciding factors for the interfacial energy released during coarsening.

The fraction of the total driving force, P, used for the primary cells is calculated from the equation of Cahn (8),

$$P = \frac{3}{\sqrt{A}} \tanh\left(\frac{\sqrt{A}}{2}\right) - \frac{1}{2} \operatorname{Sech}^2\left(\frac{\sqrt{A}}{2}\right) \qquad (40)$$

where,

$$A = \frac{K\, V_1 S_1^2}{D_b\, \delta}$$

The other equation used to calculate P is that of Petermann and Hornbogen (7)

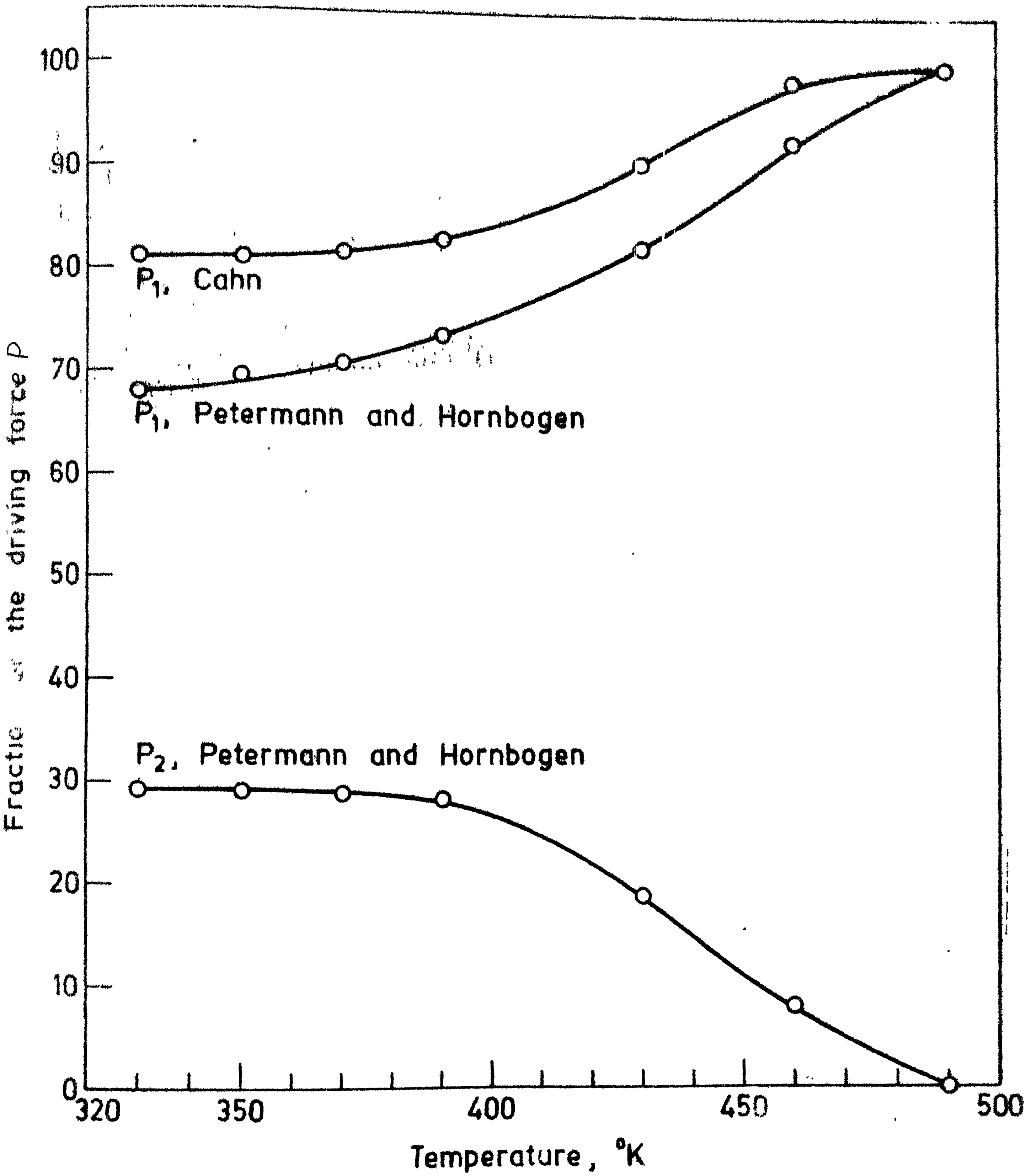
100
90
80
70
60
50
40
30
20
10
0
320
350
400
450
500
Temperature, °K
Fractic the driving force P
P1, Cahn
P1, Petermann and Hornbogen
P2, Petermann and Hornbogen

Fig. 14

TABLE 6 : Mobility and Fraction of the Driving Force Data during Primary and Secondary Reaction

T°K	M (Primary) $x10^{17} M^4 J^{-1} S^{-1}$	M (Secondary) $x\ 10^{18} M^4 J^{-1} S^{-1}$	P_1 (Primary)		P_2
			P&H	- Cahn	
490	161	50.15	1.00	-1.00	0
460	124	26.84	0.9285	0.97	0.079
430	104	20.87	0.821	0.91	0.185
390	64.5	4.85	0.735	0.85	0.263
370	23.7	1.813	0.706	0.83	0.286
350	8.2	0.95	0.695	0.82	0.289
330	2.4	0.676	0.68	0.82	0.290

$$P_1 = \frac{\Delta G_1}{\Delta G_o} \tag{41}$$

$$P_2 = \frac{\Delta G_2}{\Delta G_o} \tag{42}$$

where ΔG_1 and ΔG_2 are the chemical free energies of Primary and secondary reaction. Figure (14) shows a plot of P, using Cahn's equation for primary reaction, against T. It is observed that the values of P obtained by Cahn's analysis are slightly higher than those obtained using the analysis of Petermann and Hornbogen. Table (6) gives the values of P_1 and P_2 calculated at different temperatures. At 49°K the value of P_1 the curves is equal to 100%. The shape of the curve obtained by Petermann and Hornbogen's analysis is strongly dependent on the values of ΔG_o and ΔG_p. The values of P_1 range from 0.68 to 1.0 and the secondary values of P_2 range from 0 to 0.29. It is to be noted that the sum of P_1 and P_2 are almost equal to unity at all temperatures of ageing.

3.7 Morphology of the Cellular Reaction Products

The morphology of the Primary and secondary precipitates are shown in Figures (15) and (16). Fig.(17) shows the as quenched microstructure consisting of undecomposed α_o grains. It is observed that the supersaturated solid solution of an Al-Zn alloy decomposes at room temperature to a

depleted matrix of the same crystal structure and solute rich β phase. This is illustrated in Fig.(18). Fig.(18a) shows the microstructure of the alloy aged at room temperature, (310°K) for 7200 seconds (2 hrs). The ageing has resulted in significant grain boundary precipitation. The photomicrograph shows 2 neighbouring boundaries having the precipitate phase on grain boundaries.

In order to illustrate the growth of the grain boundary precipitate by grain boundary migration the quenched sample was aged at room temperature (310°K). A particular grain boundary region was chosen and the growth of the precipitate was studied at periodic intervals until impingement. Care was taken initially to choose a mobile boundary. The photomicrographs shown in Figures (18a,b,c,d,e,f) clearly illustrate the growth of the grain boundary precipitate through the migration of the boundary. An interesting observation from this Fig.(18) is that the curvature of the boundary changes significantly.
geing. As the ~~agency~~ ageing proceeds the bowing of the boundary is clearly illustrated in Fig.18, till the impingement occurs. As the interlamellar spacing is very fine at this temperature they could not be resolved in the optical microscope.

The mechanism for the initiation of cellular precipitate was first proposed by Tu and Turnbull (14). The details of the mechanism were discussed earlier. In this study, attempts were made to explore the possibility of orientation relationship

between α and β phases. However, it is observed that there is no definite orientation relationship between the α and β lamellae. Vijaylakshmi et.al. (29) found that during the growth of the cells the lamellae maintained orientation relationship across their interface which is as follows:

$$\{111\}_\alpha \parallel \{10\bar{1}1\}_\beta .$$

However, it is also reported that the zinc lamellae in a single colony changed their orientations frequenty without confining to a specific habit plane. Ju and Fournelle observed in their study, that cells initiated at the grain boundaries by a boundary bowing mechanism. They also found that there was no definite habit plane for the β lamellae in the α phase.

Growth of the cellular precipitate from sample quenched and aged at 187°C for time intervals of 20,25 and 30 minutes respectively,is illustrated in Fig.(19). It can be clearly seen from the micrographs that the volume fraction of the β phase increases steadily with ageing time. The Fig.(15) shows the lamellae of the cellular precipitate of the primary reaction resolved at a high magnification. The β lamellae are straight and branch out in different directions. The branching out of the lamellae is shown in Fig.(16).

The morphological features of the product of the secondary reaction are illustrated in the TEM ~~optical~~ photo-~~micro~~graph~~s~~ of Fig.(16), which show the formation of coarse

lamellae at the cell interfaces. This mechanism which requires the creation of mobile grain boundary when the primary cells intersect is found to occur frequently at lower ageing temperatures. Another mechanism proposed for the mechanism of the initiation of secondary cells is the 'S' mechanism. Fig.(16) is an illustration of the modified, 'S' mechanism. The secondary precipitate is found to be on both sides of the boundary. However, the other side is not clearly seen in the photomicrograph.

It is clear from observing the photomicrographs that the initiating mechanism for secondary are:

1. At the original α grain boundaries
2. At the impinged region of the 2 advancing fronts.

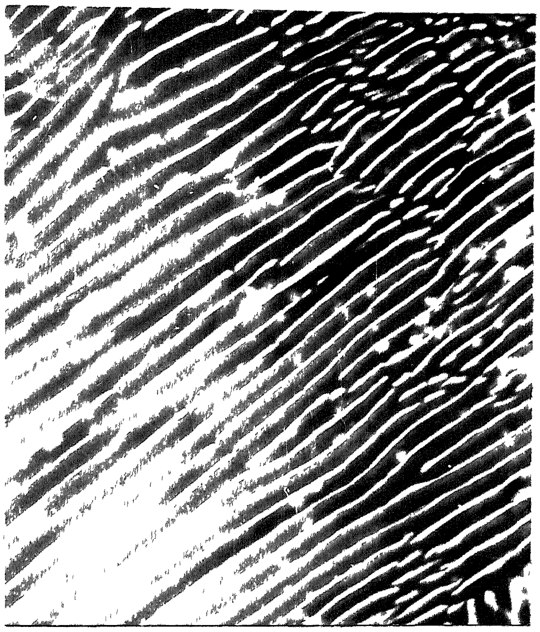

Fig.15 : T.E.M. Photograph of Primary Lamellae
Magnification = 18900
Temperature of ageing = 390°K

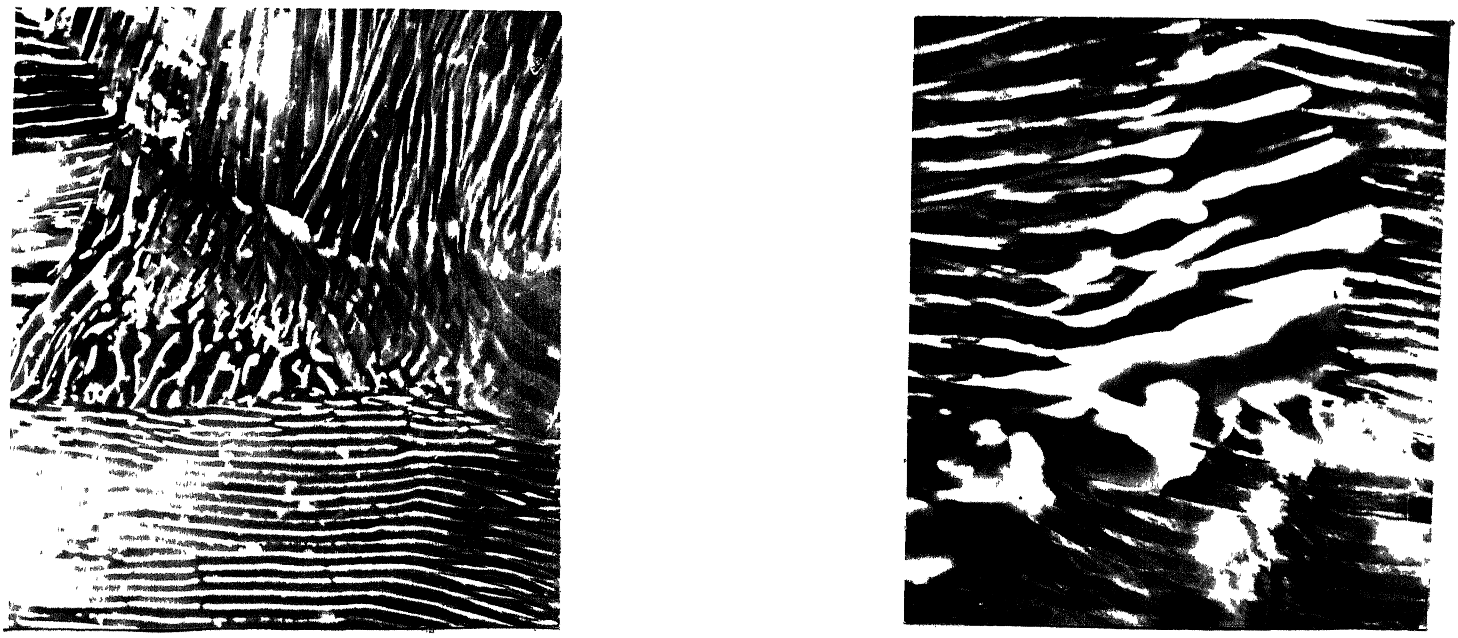

11700x

23400x

Fig.16 : T.E.M. photograph of secondary lamellae
Magnification =
Temperature of ageing = 39●°K

Fig. 17 : Microstructure of as quenched sample
Magnification = 400x

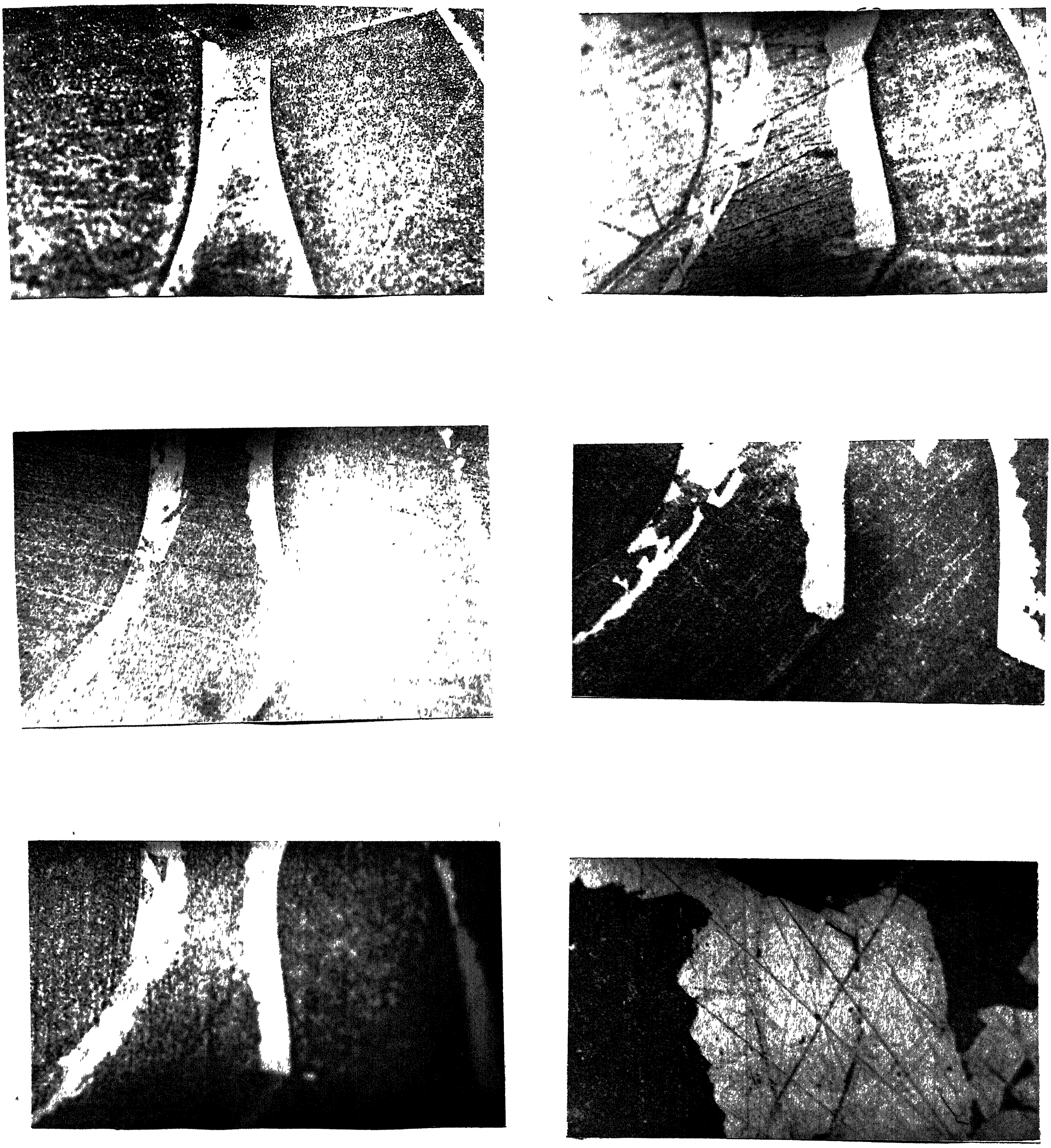

Fig. 18 : Room temperature ageing sequence of a quenched sample
Magnification = 400x

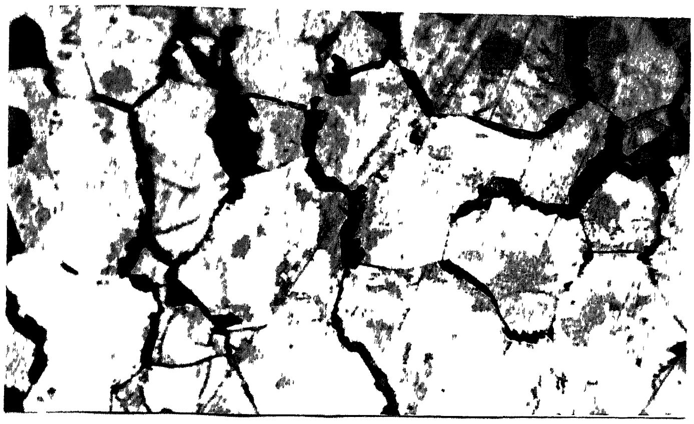

a. 20 minutes

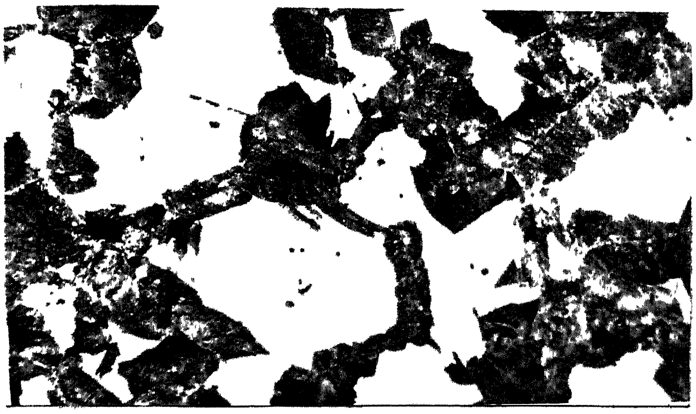

b. 30 minutes

c. 40 minutes

Fig. 19 : Formation of grain boundary precipitate
Magnification = 160X
Temperature of ageing = 460°K.

CHAPTER 4

CONCLUSIONS

The phenomenon of cellular precipitation and discontinuous coarsening was found to occur in Al-20 at % Zn alloy in the temperature range 300°K to 500°K. The cellular precipitation and coarsening process is controlled by the migration of the grain boundary.

The growth rates of the primary reaction are higher by more than an order of magnitude than the secondary reaction. The rate controlling process is the transfer of zinc through the boundary.

The interlamellar spacing of primary and secondary cells are increased with increase in the temperature of ageing. It is also seen that the Zener relationship ($S(\Delta T)^{-1}$ = constant) is valid for this alloy system.

The composition of zinc in the depleted matrix for the Primary reaction decreases as the temperature of ageing is increased. This behaviour is different from the regular shape of the solvus curve in other alloy systems. The composition of the zinc in the depleted matrix after the secondary reaction falls close to the equilibrium solvus of the Al-Zn phase diagram. This also shows the reaction is driven to near equilibrium state during secondary reaction by utilising the supersaturation after the Primary reaction.

The total driving force is contributed by the degree of supersaturation and the degree of undercooling. The values of the free energy obtained indicate that as the temperature of ageing decreases the driving force is increased.

The kinetics of primary reaction was analysed using various models. It is found that the model proposed by Petermann and Hornbogen happens to be the most suitable for the Primary reaction. The models of Aaronson and Liu, Shapiro and Kirkaldy and Turnbull yield a lower value of activation energy (47 $kJmole^{-1}$) whereas the models of Cahn, Sundquist and Petermann and Hornbogen give a value of 60 $kJmole^{-1}$. It is found out that the value of activation energy obtained by using the model of Petermann and Hornbogen falls in the range of activation energy required for the diffusion of zinc in Aluminum through the boundary. Hence, it is concluded that the rate controlling mechanism for cellular precipitation is the diffusion of zinc through the grain boundary.

The kinetics of discontinuous coarsening was analysed using the model of Petermann and Hornbogen. It is found that the data obtained in the study fits the model. The value of the activation energy is about 61 $kGmole^{-1}$ which falls in the range of activation energy for grain boundary diffusion. Hence it is seen that the discontinuous coarsening also occurs by diffusion of zinc through the grain boundary.

REFERENCES

1. R.A.Fournelle, Acta. Met., 27 (1979) 1147.
2. S.P.Gupta, To be published.
3. G.T.Partiban and S.P.Gupta, Z. Metallk, in press.
4. C.P.Ju and R.A.Fournelle, Acta. Met., 33 (1985) 71.
5. J.D.Livingston and J.W.Cahn, Acta.Met., 22 (1975) 495.
6. K.Lücke, Z. Metallk., 52 (1961) 1.
7. J.Petermann and E.Hornbogen, Z. Metallk., 59 (1968) 814.
8. J.W.Cahn, Acta. Met., 7 (1959), 18.
9. D.Turnbull, Acta. Met., 3 (1955), 55.
10. H.I.Aaronson and Y.C.Liu, Scripta, Met., 2 (1968), 1.
11. B.E.Sundquist, Metall. Trans., 4 (1973) 1919.
12. J.M.Shapiro and J.S.Kirkaldy, Acta. Met., 16 (1968) 1239.
13. C.S.Smith, Trans. AIME, 45 (1955) 533.
14. K.N.Tu and D.Turnbull, Acta. Met., 15 (1967) 369.
15. R.A.Fournelle and J.B.Clark, Met. Trans., 3 (1973) 2757.
16. E.Hornbogen, Met. Trans., 3 (1973) 2717.
17. G.Meyrick, Scripta. Met., 10 (1976) 649.
18. G.R.Speich, Trans. AIME., 242 (1968) 1359.
19. A.S.M. Metals Reference Book, (1981).
20. R.A.Fournelle, Acta. Met., 27 (1979) 1135.
21. R.D.Garwood and A.D.Hopkins, J. Inst. Metals, 81 (1952) 407.
22. K.Krishna Rao and H. Herman, J. Inst. Metals, 94 (1966), 420.

23. . K.Krishna Rao, L.E.Kaltz and H.Herman, Mater. Sci. Engg., 1, (1966-1967) 263.

24. . J.Ardell, K.Nutall and R.B.Nicholson, The mechanism of phase transformations in crystalline solids, Inst. of Metals, London (166), 22.

25. U.K.Malhotra and K.B.Rundmann, Met. Trans., 3 (1972) 1521.

26. E.P.Butler, V.Ramaswamy and P.R.Swann, Acta. Met., 21 (1973) 517.

27. T.R.Ananthraman, V.Ramaswamy and E.P.Butler, J. Mater. Sci., 9 (1974) 240.

28. K.B.Rundmann and J.E.Hilliard, Acta. Met., 15 (1967), 1025.

29. M.Vijaylakshmi, V.Seetharaman and V.S.Raghunathan, Acta. Met., 30 (1982) 1156.

30. M.Vijaylakshmi, V.Seetharaman and V.S.Raghunathan, Mater. Sci. Engg., 52 (1982) 249.

31. W.Gust, Conference Phase Transformation in Solids, Mater. Res. Soc. (1983).

32. W.J.Helfrich and R.A.Dodd, Trans. Am. Inst. Min. Engrs., 224 (1962) 557.

33. J.E.Hilliard, B.L.Averbach and M.Cohen, Acta. Met.,2(1954) 621.

34. J.E.Hilliard, B.L.Averbach and M.Cohen, Acta. Met., 7 (1959), 86.

35. D.Cheetham and F.R.Sale, Acta. Met., 22 (1974) 333.